Morphodynamic modeling and morphological upscaling in a fine sediment system

Mathew, Rooni; Winterwerp, Johan C.

DOI
10.1016/j.advwatres.2022.104224

Publication date
2022

Document Version
Final published version

Published in
Advances in Water Resources

Citation (APA)
Mathew, R., & Winterwerp, J. C. (2022). Morphodynamic modeling and morphological upscaling in a fine sediment system. *Advances in Water Resources*, *166*, Article 104224. https://doi.org/10.1016/j.advwatres.2022.104224

Advances in Water Resources 166 (2022) 104224

Contents lists available at ScienceDirect

Advances in Water Resources

journal homepage: www.elsevier.com/locate/advwatres

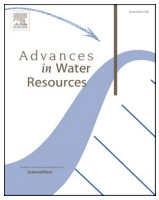

Morphodynamic modeling and morphological upscaling in a fine sediment system

Rooni Mathew [a,b,*], Johan C. Winterwerp [a]

[a] Department of Civil Engineering and Geosciences, Delft University of Technology, PO Box 5048, Delft, GA 2600, the Netherlands
[b] CDM Smith, 14 Wall St, Suite 4G, New York, NY 10005, USA

ARTICLE INFO

Keywords:
Morphological acceleration
Morphodynamic modeling
MORFAC
Fluff layer
Fine sediment

ABSTRACT

Sediment mobility and memory effects distinguish transport and morphodynamics in fine sediment settings from sandy settings. This paper focuses on the morphodynamic modeling of fine sediment systems, and an adaptation of modeling procedures more commonly used in sand-dominated systems. An extensive dataset of short-term transport and morphological trends along with ancillary data is used to support the development, parameterization, and calibration of a morphodynamic model of the Lower Passaic River (USA). The model is subsequently extended to include a morphological acceleration procedure in order to enable computationally efficient morphodynamic simulations. The performance of the resulting model is first verified and subsequently validated using measured decadal-scale morphological change. Subsequently, the model is used to assess the current morphodynamic status and the long-term response of the river to forcings such as shipping, episodic storm events, and climate change, with results that are consistent with theoretical expectations.

1. Introduction

The morphological evolution of estuaries is of consequence for problems such as contaminant fate and transport, water quality, siltation of navigation channels, dredged material management, impact of engineering works, etc. Morphological change is a function of the bed-water exchange processes of erosion and deposition, and the water column transport processes of advection and dispersion. These processes are often parameterized and simulated in process-based numerical morphodynamic models for an assessment of morphological response to external forcings or to engineering works. Such morphodynamic models have been developed and applied more commonly in sand-dominated[1] systems (Lesser et al., 2004; Roelvink, 2006) than in fines-dominated systems (Vested et al., 2013), likely due to the site-specific, spatially--variable, and temporally-variable nature of various fine sediment transport processes that typically requires extensive data for representation and parameterization in numerical models. This paper focuses on the morphodynamic modeling of fine sediment systems, and the adaptation of modeling procedures more commonly used in sand-dominated systems. However, there are important differences between sand and fine sediment transport that require examination in the context of process-based morphodynamic models.

Sand transport is typically an equilibrium process characterized by capacity load conditions, i.e., an equilibrium exists between the (local) sediment load and the transport capacity of the (local) turbulent flow velocity. As this equilibrium is rapidly established under alluvial bed conditions, morphological change in sandy settings is a function of gradients in transport and is generally calculated using equilibrium transport formulations (van Rijn, 1993), although pick-up functions for prescribing bed-water exchange processes may be used as well. In contrast, fine sediment transport is typically characterized by non-equilibrium conditions with respect to the carrying capacity of the flow. The non-equilibrium behavior can originate from beds comprised of a mixture of sands and fines (thus limiting the erosion of fines), beds with a vertical gradient in erodibility[2] (thus limiting erosion under given shear stress), or systems where settling velocities are too low to achieve

* Corresponding author at: Department of Civil Engineering and Geosciences, Delft University of Technology, PO Box 5048, Delft, GA 2600, the Netherlands.
E-mail address: mathewr@cdmsmith.com (R. Mathew).

[1] Sand and fine-sediment are nominally defined as particle sizes greater than and less than 63 μm, respectively. Moreover, we implicitly assume that fines exhibit cohesive behavior.

[2] Erodibility in the context of this paper refers to the critical shear stress for erosion, τ_{Cr}, the threshold bed shear stress required to be exceeded for surface erosion to occur following the Partheniades erosion formulation (Partheniades, 1965). An increase in the critical shear stress for erosion with depth represents a decrease in sediment erodibility with depth.

https://doi.org/10.1016/j.advwatres.2022.104224
Received 21 April 2021; Received in revised form 10 May 2022; Accepted 17 May 2022
Available online 27 May 2022

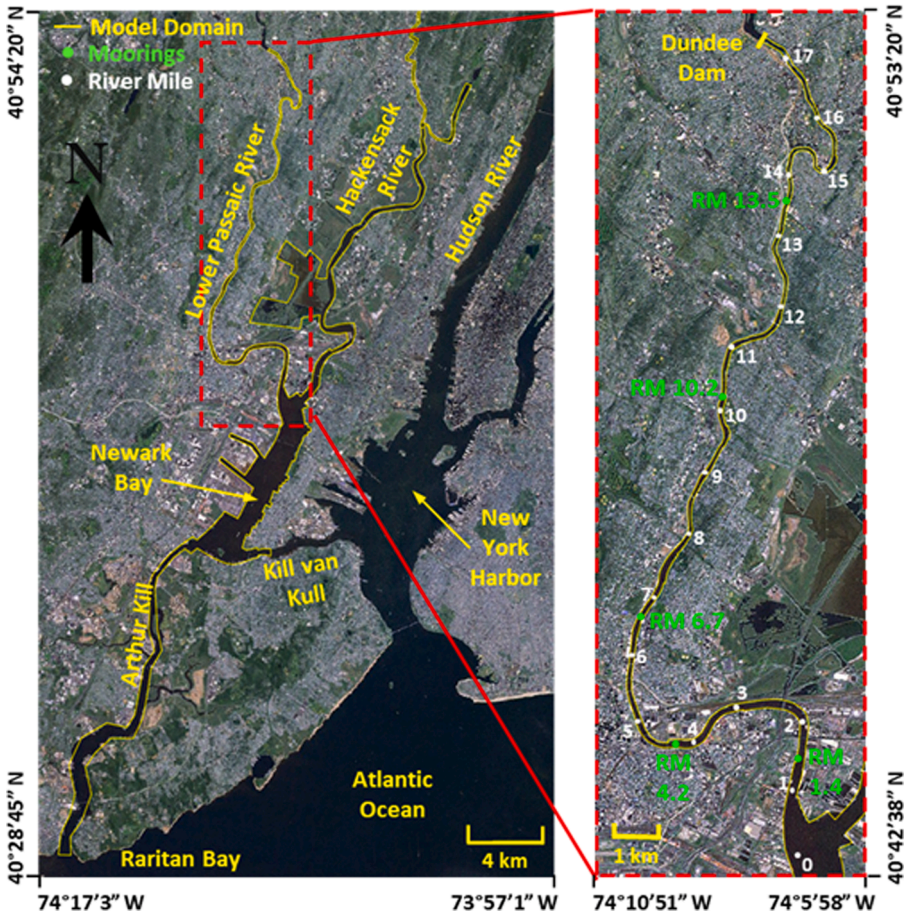

Fig. 1. Location map of the lower Passaic river along with the locations of in situ moorings and outline of model domain.

significant deposition of fines (thus limiting sediment availability for erosion); these are referred to as supply-limited, erosion-limited, or settling-limited conditions, respectively (Winterwerp et al., 2021). Such phenomena control local bed-water exchange, and consequently, gross erosion and gross deposition have to be modeled explicitly through pick-up and deposition functions rather than with equilibrium transport formulations.

Related to the notion of erosion-limited transport is the effect of armoring, stratification, and consolidation of the sediment bed in causing a decrease in erodibility with depth (Mehta, 1988; Sanford and Maa, 2001). This implies that the amount of mobile sediment (i.e., sediment available for erosion under given flow regime) and morphological response to a given event is not only a function of the event magnitude but also the time-history of events (Vested et al., 2013; Mathew and Winterwerp, 2020). Erosion-limited transport can be manifest during non-event (e.g., tide-dominated) conditions when erosion may be limited to a thin layer (thickness on the order of millimeters) of easily-erodible surficial sediments termed the fluff layer (Mathew and Winterwerp, 2017), during episodic events (e.g., high river flow) when erosion may extend deeper into the bed, as well as during intermediate conditions (e.g., low-moderate river flows) when erosion is limited to the fluff layer but transport (from the head-of-tide) is important for sediment supply considerations (Winterwerp et al., 2021; Mathew and Winterwerp, 2020). Thus, the system develops a memory (represented by the availability of mobile sediment), affected largely by past conditions and events, that influences subsequent morphological development. The sediment mobility and memory effects steer morphological development on short (tidal time-scales) and long time-scales (many years) by influencing erosion (and deposition in case the eroded sediment were to be deposited elsewhere in the system). Consequently, morphodynamics in fine sediment settings can be non-linear, i.e., becoming poorly related to the instantaneous event magnitude. This poses challenges for the morphodynamic modeling of such systems, beyond those encountered in sandy systems.

Typically, morphodynamic models for sandy systems are based on sediment transport models calibrated to site-specific data for relatively short-term periods, and then used to perform long-term simulations. Therefore, the first objective of this paper is to investigate whether a similar procedure (of developing a morphodynamic model calibrated over relatively short-term periods) may be applied in erosion-limited, fine sediment settings where memory effects are prominent. We start from a mixed (sands and fines) sediment transport model, calibrated over a range of hydrologic conditions and using various calibration metrics. The model is then run in morphodynamic mode, prescribing all hydrodynamic forcing in detail – we refer to brute-force morphodynamic simulations over the timescale of a few years, with model performance assessed using measured morphological change. This is similar to the setup of morphodynamic models for sandy systems.

Further to morphodynamic modeling in sandy systems, recent advances in this subject area include the morphological acceleration factor (Morfac) technique for morphodynamic upscaling which enables morphological simulations over extended time-scales in a computationally efficient fashion (Lesser et al., 2004; Roelvink, 2006; Ranasinghe et al., 2011; Lesser, 2009). The Morfac approach has been successfully applied in sandy systems over multi-year to millennial time-scales by various authors (van der Wegen and Roelvink, 2008; Dam et al., 2016; Styles et al., 2016). Although not as extensively applied as for sandy systems, the Morfac approach has also been applied to fine sediment systems (Ganju et al., 2009; George et al., 2012; van der Wegen and Jaffe, 2014). However, as it is not obvious that the Morfac

approach can yield realistic results for fine sediment systems with memory effects at all time scales, the second objective of this paper is to investigate the viability of the Morfac approach for decadal-scale morphodynamic simulations in erosion-limited fine sediment settings. Subsequently, the morphodynamic model using Morfac is used to address specific research questions related to long-term morphodynamics.

Accordingly, the paper is divided into three major parts. The first part describes the development and calibration of the morphodynamic model (over the timescale of a few years) for the particular estuary presented here; a calibrated model is necessary for the Morfac approach described in the second part of the paper. The second part includes a comparison of results from the morphodynamic model with Morfac to the brute-force simulations in order to test the applicability of the Morfac approach in fine sediment settings. As additional validation of the Morfac approach over the long-term, the second part also compares the performance of the morphodynamic model with Morfac to decadal-scale data for morphological change. Finally, the third part of the paper presents the application of the morphodynamic model with Morfac to assess long-term morphodynamic response to various system forcings that cannot otherwise be determined empirically. These include the role of navigation, which is specific to the particular estuary presented here, the role of episodic storm events, and the impact of climate change. The following sections present an overview of morphodynamics in the particular estuary that is the subject of the model application presented here, followed by the afore-mentioned three major parts of the paper and a discussion.

2. Site overview and sediment dynamics

The data presented in this manuscript come from the Lower Passaic River (LPR), an estuary that is part of New York Harbor, USA (Fig. 1). The data presented here were collected as part of an ongoing environmental cleanup effort of the LPR. The LPR stretches approximately 28 km long from its mouth in Newark Bay at River Mile (RM) 0, to the head-of-tide at Dundee Dam (RM 17.5). Newark Bay is connected to New York Harbor and Raritan Bay (and the Atlantic Ocean) via the tidal inlets Kill van Kull and Arthur Kill, respectively. The width of the LPR ranges from approximately 600 m at its mouth, declining to about 200 m at RM 1.4, 150 m at RM 4.2, 120 m at RM 6.7, 90 m at RM 10.2, and 75 m at RM 13.5, i.e., locations about 1.5 km, 6 km, 10 km, 15.5 km, and 21 km, respectively, from the mouth of the river. These were also the locations of months-long (October 10, 2009 to December 16, 2009, and March 22, 2010 to July 24, 2010) in situ measurements of salinity, velocity, water depth, and suspended sediment concentrations (SSC) used to calibrate the numerical model presented here. Typical water depths along the thalweg in the LPR currently range between 5 and 7 m (with respect to mean sea level; MSL). The LPR is characterized by the remnants of a navigation channel dredged several decades ago (design depths of about 10 m at the mouth and 4 m in the upper reaches) but no longer actively maintained.

The hydrodynamics and sediment dynamics in the LPR were analyzed by Mathew and Winterwerp (2020) using the in situ data and are summarized here; these dynamics represent the conceptual model of sediment transport used to support the development of the morphodynamic model in the following sections. The primary hydrodynamic forcings within the LPR include barotropic and baroclinic circulation, and river flow. Barotropic circulation includes the periodic tide as well as episodic coastal setup/setdown events, both of which result in volume fluxes into and out of the estuary driven by the along-channel water level gradient. Semi-diurnal tides (period of 12.42 h, corresponding to the dominant semi-diurnal M_2 constituent, and tidal range of 0.9 to 2.1 m from neap to spring) entering Newark Bay through the Kill van Kull and Arthur Kill propagate to the LPR and the head-of-tide at Dundee Dam. Baroclinic circulation is induced by along-channel density gradients resulting from the mixing of freshwater from the head-of-tide, and saline water from the ocean. The resulting longitudinal salinity gradient induces residual near-bottom currents directed up-estuary and near-surface currents directed down-estuary. Salinity intrusion occurs under most river flows (annual average river flow at Dundee Dam is about 34 m^3/s), with the saline water flushed out of the LPR at high river flows (>200 m^3/s; return period of 2 years). The extent of salinity intrusion, as indicated by the location of the salt front, also determines the location of the estuarine turbidity maximum (ETM), a zone of elevated SSC and enhanced sediment trapping.

Suspended sediment transport in the LPR varies over tidal timescales, responding to the cyclic variations in tidal currents by eroding and replenishing (by deposition) the sediment inventory in the fluff layer. The presence of the fluff layer in the LPR has been observed in erodibility measurements using a Gust Microcosm on shallow sediment cores, as well as other lines of evidence (Mathew and Winterwerp, 2017). Briefly, the Gust Microcosm experimental setup consists of an enclosed chamber containing a sediment core overlaid by a layer of continually refreshed water. A sequence of increasing shear stresses is imposed by varying the rotation speed of a disc positioned above the water and the sediment mass eroded at given shear stress is measured. The erosion rate and shear stress measurements are subsequently analyzed to determine the profile of τ_{Cr} over a relatively shallow depth interval (on the order of mm). The data show a thin pool (2–4 mm thick) of easily erodible sediments overlying less-erodible strata and comprised of sediments that are resuspended twice every tidal cycle (once during flood and again during ebb) and redeposited around slack water. Increasing river flow alters these dynamics in two respects – by preventing deposition around slack water (i.e., preventing replenishment of the fluff layer), and by causing erosion of the more consolidated sediments underneath the fluff layer. Consequently, sediment transport, as inferred from the tidally integrated net suspended sediment flux (SSF), is influenced by barotropic and baroclinic circulation, with the magnitude and direction of SSF modulated by river flow. During low river flow, lag effects and tidal asymmetries induced by barotropic processes, and baroclinic circulation induced by salinity intrusion and mixing result in net up-estuary transport of sediment. Increasing river flow reduces the influence of these up-estuary transport pathways, delivers additional sediment loading from the head-of-tide, causes erosion, and results in net down-estuary SSF.

Conceptually, sediment dynamics in the LPR follows one of three regimes depending on river flow at any given time – importing, flushing, scouring (Mathew and Winterwerp, 2020). In general terms, low river flow conditions are associated with net up-estuary SSF and represent an importing regime (Regime I), and conversely, increasing river flow is associated with net down-estuary SSF and export of sediment from the system. The exporting regime can be further distinguished into two conditions, distinguished by morphological impact – flushing conditions, thus referred to since only (mainly) the sediments within the fluff layer are eroded (Regime II), and scouring conditions, thus referred to since the more consolidated layers underneath the fluff layer are eroded (Regime III). In other words, during low-to-moderate river flows (Regimes I and II), erosion is limited to the fluff layer, and only during high river flows (nominally Regime III), are shear stresses high enough to cause erosion of the less-erodible strata underlying the fluff layer (Mathew and Winterwerp, 2020). Although variable locally, for the system as a whole, the river flow rate thresholds between Regimes I and II and between Regimes II and III are approximately 20–30 m^3/s and 200 m^3/s, respectively. This implies that sediment transport in the LPR is dominated by fluff layer dynamics, i.e., erosion-limited, the majority of the time. The availability of sediments in the fluff layer is responsible for the net transport of fine sediments by barotropic and baroclinic circulation against the direction of residual (river) flow. Therefore, the infill of the estuary with fines from down-estuary is governed by the fluff layer dynamics (Mathew and Winterwerp, 2020) which therefore needs to be accounted for in the morphodynamic model.

The general process of sediment import during low river flow periods

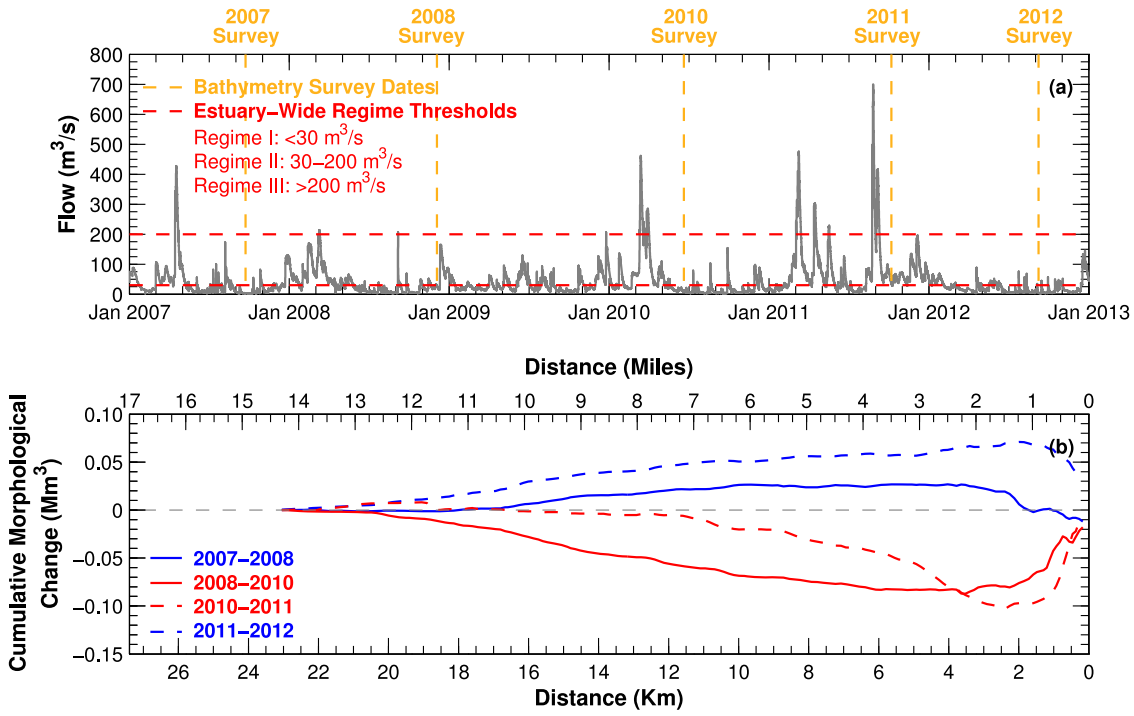

Fig. 2. Time-series of (a) measured flow rate at the head-of-tide in the LPR over the period of the bathymetry surveys, and (b) measured longitudinal profile of cumulative (in the seaward direction) volumetric morphological change in the LPR with positive and negative slopes indicating deposition and erosion, respectively.

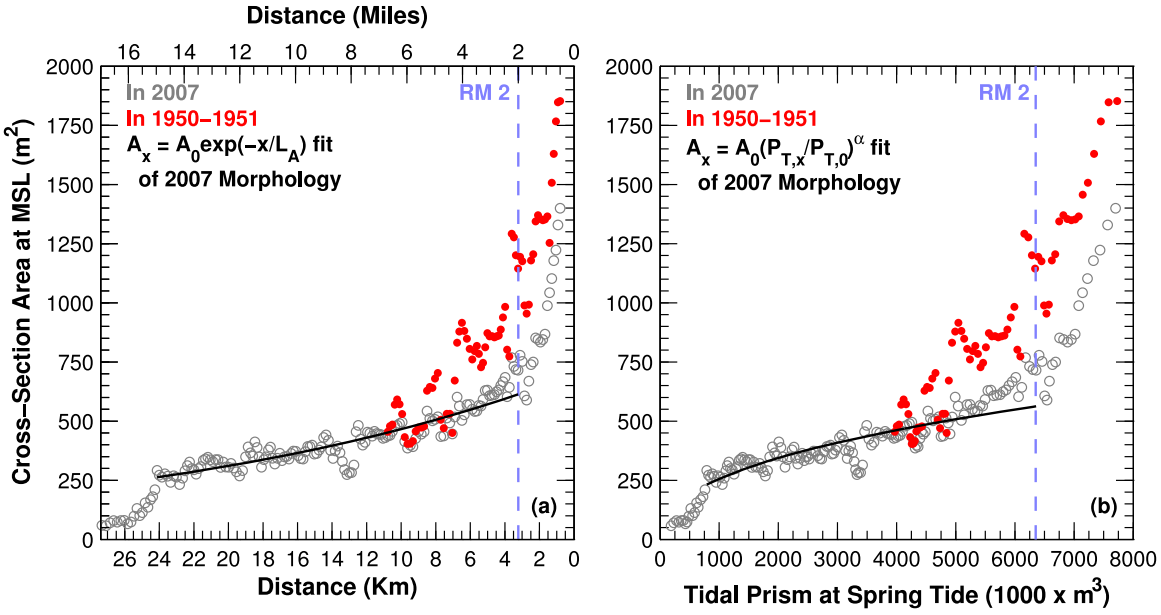

Fig. 3. Relationship of submerged cross-sectional area (at MSL) with (a) distance along the river and (b) with tidal prism at spring tide. Cross-section area based on bathymetry in 2007 and 1950–1951. Tidal prism calculated using the numerical hydrodynamic model described in this paper.

and export during high river flow periods is also apparent in the morphological change measured in a series of inter-annual multi-beam bathymetric surveys performed in September 2007, November 2008, June 2010, October 2011, and September 2012 (Mathew and Winterwerp, 2020). The along-channel cumulative volumetric change between consecutive surveys is shown in Fig. 2 along with the river flow rate during this five-year period. River flow ranged from a low of about 1 m^3/s in October 2007, to highs of 450 m^3/s in March 2010 and March 2011 (return period of 25 years), and 700 m^3/s in August 2011 (return period of 90 years). The periods between the 2007–2008 and 2011–2012 surveys represent relatively low-flow conditions, with generally Regimes I and II events whereas the periods between the 2008–2010 and 2010–2011 surveys included several Regime III events and represent relatively high-flow conditions. The impact of the varying flow regimes is apparent in the measured morphological change, with different behavior for the reaches seaward and landward of RM 2. Landward of RM 2, the low-flow periods (2007–2008 and 2011–2012) experienced deposition whereas the high-flow periods (2007–2008 and 2011–2012) experienced erosion. The 2010–2011 period experienced erosion at locations further seaward than the 2008–2010 period, an

Table 1
Parameter values for the hydrodynamic and sediment transport models.

Parameter	Value
Bottom roughness, z_0 (mm)	1
Coefficient in Smagorinsky horizontal turbulence closure scheme	0.01
Fluff and transition layer thickness (mm)	2
Channel, Fluff and transition layer erosion rate coefficient, M (kg/m^2/Pa/s)	5×10^{-4}
Channel, Fluff layer critical shear stress, τ_{Cr} (Pa)	0.03
Channel, Transition layer critical shear stress, τ_{Cr} (Pa)	0.2
Shallows, Fluff and transition layer erosion rate coefficient, M (kg/m^2/Pa/s)	1.5×10^{-3}
Shallows, Fluff layer critical shear stress, τ_{Cr} (Pa)	0.01
Shallows, Transition layer critical shear stress, τ_{Cr} (Pa)	0.07
Consolidated layers, thickness at bed surface (mm)	25
Consolidated layers, critical shear stress at bed surface, τ_{Cr} (Pa)	0.5
Consolidated layers, critical shear stress at depth in bed, τ_{Cr} (Pa)	1.8
Consolidated layers, for $\tau_b = 0.5$ — 2 Pa, erosion rate at bed surface, E (mm/s)	2.5×10^{-3} — 7.8×10^{-2}
Consolidated layers, for $\tau_b = 0.5$ — 2 Pa, erosion rate at depth in bed, E (mm/s)	1×10^{-4} — 3.2×10^{-3}
Critical shear stress for deposition, τ_{Dep} (Pa)	∞
Settling velocity of poorly-flocculated fines (mm/s)	0.20
Settling velocity of flocculated fines (mm/s)	0.40
Settling velocity of bed fines (mm/s)	0.80

observation that is consistent with the greater magnitude of river flow during the former period. In addition, effects of bed armoring are apparent in the morphological change over 2010–2011. Specifically, the reach landward of RM 7 does not show significant erosion during 2010–2011 which is in contrast to the significant erosion in this reach during 2008–2010. It is likely that a highly consolidated fine sediment layer and/or armoring by coarser sediment exposed during the Regime III event in 2008–2010 prevented further erosion in 2010–2011. Such erosion-limited behavior therefore needs to be accounted for in the morphodynamic model. In contrast, the reach seaward of RM 2 experienced deposition during the high-flow years because of the increasing river cross-section and relatively low shear stress regime in these areas (as compared to the relatively high shear stress regime in the more landward locations that experienced erosion), and experienced erosion during the low-flow years because of the impact of ongoing shipping (Mathew and Winterwerp, 2020). This reach contains several active shipping terminals (U.S. Army Corps of Engineers, 2010), and as explained subsequently, shipping-induced scour maintains a state of dynamic morphological equilibrium that is different than would be expected under natural conditions. Review of bathymetry data in the vicinity of the shipping terminals shows accretion in these areas during high-flow years, followed by erosion and a return to a near-equilibrium bathymetry under mean conditions.

The current morphodynamic status of the LPR is apparent from an assessment of two common morphodynamic relationships (longitudinal convergence of river cross-section, and tidal prism to cross-section relation (Winterwerp et al., 2021; D'Alpaos et al., 2010) as shown in Fig. 3. Tidal prism is defined as the volume of water entering the estuary during the flood phase of the tide (in the absence of any freshwater inflows, this is the volume of water leaving the estuary during the ebb phase of the tide). These relationships are also used subsequently to interpret the results of the prognostic assessments of the impacts of navigation, episodic storm events, and climate change. Between RM 2 and RM 15, the LPR currently conforms to the following trends:

- An exponentially converging form – given the cross-sectional area A_x at given location x, and the relationship $A_x = A_0\exp(-x/L_A)$, the reference cross-section at RM 2, A_0, is calculated as 615 m^2, and convergence length, L_A, as 24.7 km. This indicates that even though the river was modified in the past (e.g., dredged for navigation, shorelines hardened, and inter-tidal wetlands reclaimed), it has regained an exponential cross-section distribution.
- A relationship between the cross-section area and tidal prism – given the cross-sectional area A_x and tidal prism at given location $P_{T,x}$, and the relationship $A_x = A_0(P_{T,x}/P_{T,0})^{\propto}$, the reference cross-section at RM 2, A_0, is calculated as 560 m^2, and the exponent, $\propto$, as 0.43. The exponent is typically in the range of 0.85–1.1 in tidal inlets (D'Alpaos et al., 2010). The reason for the lower value noted in the LPR is further explored subsequently.

Seaward of RM 2, the river cross-section increases, and the relationship with tidal prism changes; the reason for this is related to the morphological impact of shipping which is explored subsequently. As mentioned previously, the LPR was dredged for navigation purposes historically, with the last major dredging events occurring in 1950–1951 (between RM 0 and RM 6.7), and in 1983 (between RM 0 and RM 1.5) (U.S. Army Corps of Engineers 2010). Comparison of the post-dredging and current cross-sections in Fig. 3 shows the morphodynamic response of the river to the disequilibrium caused by dredging, with significant infilling between RM 0 and RM 6.7. This infilling was likely a combination of sediment deposited during Regime III events, and sediment transported up-estuary during Regime I and II conditions. The larger river cross-sections historically also imply that sediment trapping efficiency has decreased over time in response to the evolving morphology.

The availability of data describing short-term and long-term morphological change, along with data for parameterizing and calibrating a numerical model therefore provides opportunity for developing a morphodynamic model of the LPR calibrated to multiple lines of evidence. The conceptual model of sediment dynamics (the three transport regimes, erosion-limited transport, fluff layer dynamics) described in this section was therefore used as the basis of the morphodynamic model of the LPR, and subsequently, for development of the Morfac approach.

3. Morphodynamic model

The morphodynamic model presented here uses the Estuarine, Coastal and Ocean Model (ECOMSED) framework (Blumberg and Mellor, 1978; HydroQual Inc., 2010), which includes integrated hydrodynamic and sediment transport sub-models. As part of the environmental studies of the LPR, ECOMSED was used for a hydrodynamic application (HydroQual 2008) as well as a sediment transport application (Moffatt Nichol and Deltares, 2019) of the LPR. Model inputs and calibration parameters established as part of the hydrodynamic application were used in the present study. Although the sediment transport application used somewhat different formulations, some inputs such as initial conditions, erodibility inputs, boundary conditions, etc., used in the present study are based on the model application of Moffatt Nichol and Deltares (2019). The formulations and setup of the morphodynamic model is presented next followed by model performance.

3.1. Model setup

The morphodynamic model involves a three-dimensional time-variable application over a domain that includes the LPR, Hackensack River, Newark Bay, Arthur Kill, and Kill van Kull (model domain shown in Fig. 1). The spatial domain is resolved using a shoreline-fitted variable-resolution curvilinear orthogonal grid. Grid resolution in the LPR ranges from seven cells across the river at RM 1.4 and decreasing to three cells across the river at RM 13.5. Average grid resolution in the LPR is 35 m wide and 140 m long, with a ten-layer σ-coordinate system in the water column. Briefly, the three-dimensional hydrodynamic model solves a system of equations describing the conservation of mass, momentum, heat, and salt (Blumberg and Mellor, 1978; HydroQual, Inc. 2010). Vertical mixing is resolved using the second order turbulence closure scheme of Mellor and Yamada (1982), and sub-grid scale horizontal

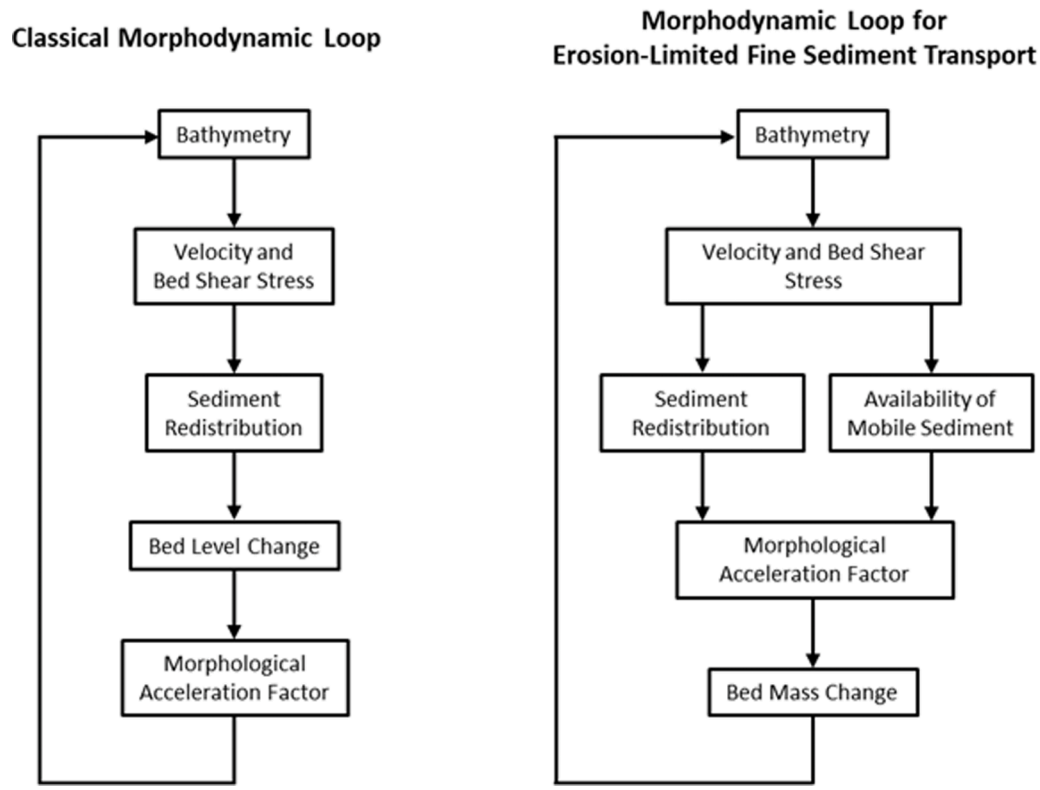

Fig. 4. Schematic of classical morphodynamic loop (for sandy settings; adapted from van der Wegen and Roelvink (2008)) and refined schematic for erosion-limited fine sediment settings.

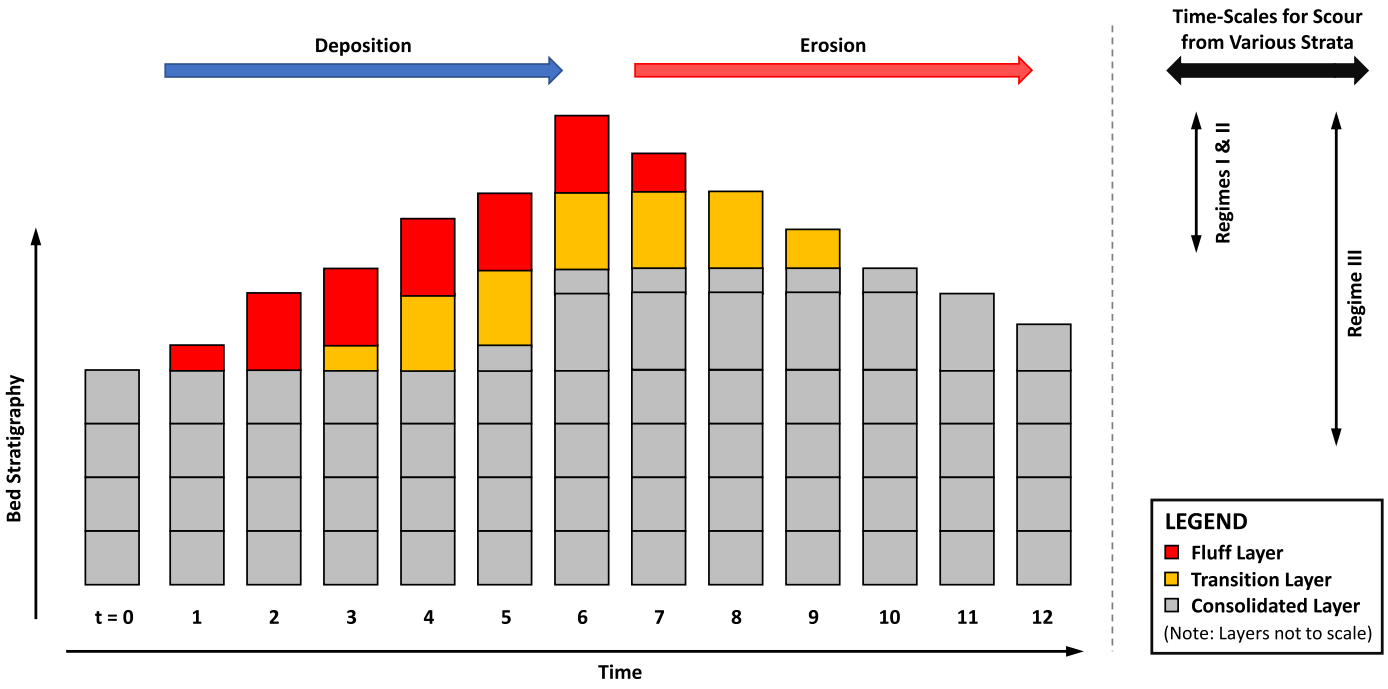

Fig. 5. Schematic of bed layering and conceptual representation of hydrodynamic conditions potentially responsible for erosion from various strata.

mixing parameterized using Smagorinsky (1963). Boundary conditions for the hydrodynamic model include the measured river flow entering from the head-of-tide in the LPR and tributaries, and the tide, salinity, and temperature at the marine boundaries (Kill van Kull and Arthur Kill; marine boundary conditions specified using the results of the regional-scale hydrodynamic model (HydroQual, 2008). The hydrodynamic model was calibrated by adjusting bottom roughness and horizontal mixing to reproduce measured water level, and three-dimensional velocity, temperature, and salinity. The calibration approach implicitly assumes that temporal changes in mud dynamics (e.g., in response to dredging, due to bed coarsening during storm events, etc.) do not affect the hydrodynamics. Table 1 provides a tabulation of

the major model parameter values.

The sediment transport module in ECOMSED calculates the advection and dispersion of suspended sediments originating from the boundaries, settling, and the bed-water exchange processes of erosion and deposition (HydroQual Inc., 2010). The three-dimensional advection-dispersion equation for suspended sediment transport is:

$$\frac{\partial C}{\partial t}+\frac{\partial UC}{\partial x}+\frac{\partial VC}{\partial y}+\frac{\partial (W-W_S)}{\partial z}=\frac{\partial}{\partial x}\left(A_H\frac{\partial C}{\partial x}\right)+\frac{\partial}{\partial y}\left(A_H\frac{\partial C}{\partial y}\right)+\frac{\partial}{\partial z}\left(K_H\frac{\partial C}{\partial z}\right) \quad (1)$$

where,C is suspended sediment concentration, U, V, and W represent velocities along the x, y, and z directions, respectively, W_S is the settling velocity, A_H is the horizontal diffusivity, and K_H is the vertical eddy diffusivity. Eq. (1) is subject to the boundary conditions $K_H\frac{\partial C}{\partial z}=0$ and $\frac{\partial (W-W_S)}{\partial z}=0$ at the air-water interface, and $K_H\frac{\partial C}{\partial z}=E-D$ and $\frac{\partial (W-W_S)}{\partial z}=0$ at the sediment-water interface, where E is the erosion rate and D is the deposition flux. As part of the present study, two key modifications were introduced to ECOMSED. The first modification, described in this section, includes the representation of a stratified bed layering scheme (with depth-dependent erodibility) that is key to sediment dynamics pertaining to erosion-limited transport and memory effects. The second modification, described in the following section, includes the implementation of morphological acceleration using Morfac.

As discussed in the preceding section, the LPR is characterized by erosion-limited transport, i.e., erosion is a function of the sediment substrate and stratigraphy. Accordingly, the classical morphodynamic feedback loop commonly used in sandy settings was modified for application to fine sediment settings as shown in Fig. 4. The primary refinement is consideration of the availability of mobile sediment in the transport formulations. Note that the morphological acceleration factor included in Fig. 4 is applicable to the analyses in the following section. The spatially and temporally varying erosion and deposition fluxes computed by the model in response to the non-equilibrium transport formulations are used to compute the changing bed stratigraphy, composition, mass, and consequently, the bed thickness. The resulting morphological change is used to update the bathymetry used for hydrodynamic calculations in the following timestep. Thus, the hydrodynamic solution adapts and self-adjusts in response to the evolving bathymetry during the simulation.

The conceptual description and quantitative parameterization of erosion-limited transport in the model is based on erodibility measurements. As mentioned previously, the sediment bed is characterized by the presence of an easily-erodible fluff layer overlying less-erodible strata (Mathew and Winterwerp, 2017). Within the fluff layer, τ_{Cr} values increase by approximately an order of magnitude. Erodibility measurements using a Sedflume device (Borrowman et al., 2006) and analyzed by Moffatt Nichol and Deltares (2019) show approximately an additional four-fold increase in τ_{Cr} over the top 30 cm of the bed. This conceptual description of depth-dependent erodibility was used as the basis for a multi-layer bed model.

Fig. 5 shows a schematic of the bed layering developed to represent the depth-dependent erodibility along with a conceptual description of the hydrodynamic conditions that can potentially scour through the various strata. The fluff layer is located at the bed-water interface and is subject to erosion and deposition. During erosional conditions (e.g., the first half of the flood tide), the fluff layer may be depleted and disappear. During the following depositional condition (e.g., the second half of the flood tide and high-water slack), depositing sediments first recreate the fluff layer. When the fluff layer exceeds its pre-determined maximum thickness, the excess sediment is transferred to the underlying layer. Given the order of magnitude difference in erodibility between the fluff layer and the underlying less erodible layer, the model includes an intermediate transition layer (with same maximum allowable thickness as the fluff layer) with intermediate strength. When both the fluff and transitional layers reach their pre-determined maximum thickness, new layers are created underneath the transitional layer, simulating consolidation. Under depositional conditions, sediment is transferred from the fluff layer through the transitional layer and to the layer underneath. Under erosional conditions, layer depletion proceeds in a logical sequence with the fluff layer eroded first, followed by the underlying layers. Erosion rate for the fluff and transition layers follows a modification of the Partheniades formulation for surface erosion:

$$E=M(\overline{\tau}_b-\tau_{Cr})\ for\ \overline{\tau}_b>\tau_{Cr} \quad (2)$$

where, $\overline{\tau}_b$ is the turbulence mean bed shear stress, and M is the erosion rate coefficient. Within the relatively deep channel, parameters τ_{Cr} and M were specified using the approach of Mathew and Winterwerp (2017) and marginally adjusted (within the estimated uncertainty limits) during calibration. However, the sub-tidal shallows outside the channel were parameterized as three times more erodible (i.e., parameters τ_{Cr} and M reduced and increased, respectively, by a factor of three) than the channel areas, primarily by calibration. Though this model describes the vertical response of the bed to erosive forcing, it basically parameterizes spatial variability within grid cells, as elaborated by Winterwerp and van Kesteren (2004).

The less-erodible layers underneath the fluff and transitional layers are treated somewhat differently. In order to enable efficient management of the bed layers, mainly with respect to depth- and time-dependent erodibility, these layers are formulated using the consolidation model of Sanford (2008). Briefly, the consolidation model prescribes an equilibrium depth-profile of bed density ρ_{eq} as:

$$\rho_{eq}=\rho_\infty-(\rho_\infty-\rho_0)\exp(-\phi O) \quad (3)$$

where, ρ_0 is the density at the bed surface, ρ_∞ is the asymptotic density at depth, O is the mass of sediment above given depth in the bed (referred to as the overmass), and ϕ is an empirical parameter. Given the equilibrium density profile, at any point in time t and depth within the bed, the instantaneous density ρ approaches equilibrium following the first-order approximation:

$$\frac{\partial \rho}{\partial t}=r_c(\rho_{eq}-\rho)H(\rho_{eq}-\rho)-r_s(\rho_{eq}-\rho)H(\rho-\rho_{eq}) \quad (4)$$

where,H is the Heaviside step function ($H=1$ when its argument is ≥ 0 and $H=0$ otherwise), r_c is the first-order consolidation rate, and r_s is the first-order swelling rate. The instantaneous depth-dependent density is related to the erosion rate using a power-law formulation (Roberts et al., 1998):

$$E=A\overline{\tau}_b{}^n\rho^m \quad (5)$$

where, A, n, and m are empirical parameters. Finally, the time- and depth-dependent τ_{Cr} is estimated by rearranging Eq. (5) such that τ_{Cr} is calculated as that shear stress which results in given critical threshold erosion rate E_{Cr} (Roberts et al., 1998). It is noted that although the effect of the abiotic swelling process on sediment erodibility is explicitly represented in the model, biological activity in the sediment (e.g., bioturbation) may also affect erodibility. This is, in part, implicitly accounted for in the model parameterization established using the combination of empirical data and calibration described next. Parameters ϕ, A, n, m, and E_{Cr} in Eqs. (3) and (5) were determined by fitting the measured density, erosion rate, and τ_{Cr} profiles (Moffatt Nichol and Deltares, 2019, Borrowman et al., 2006). Parameter r_c was estimated as 0.25 (d^{-1}) using the results of Sedflume erosion experiments on cores reconstituted in settling columns and tested at different intervals after self-weight consolidation (Sea Engineering, 2013), whereas parameter r_s was defined as $0.01r_c$ based on Sanford (2008). Although the application of the consolidation model involves the determination of several fitted parameters, the resulting metrics of interest (erosion rate, τ_{Cr}, and ρ) are constrained by measured values. The parameterization of the consolidation model results in equilibrium profiles with increasing density,

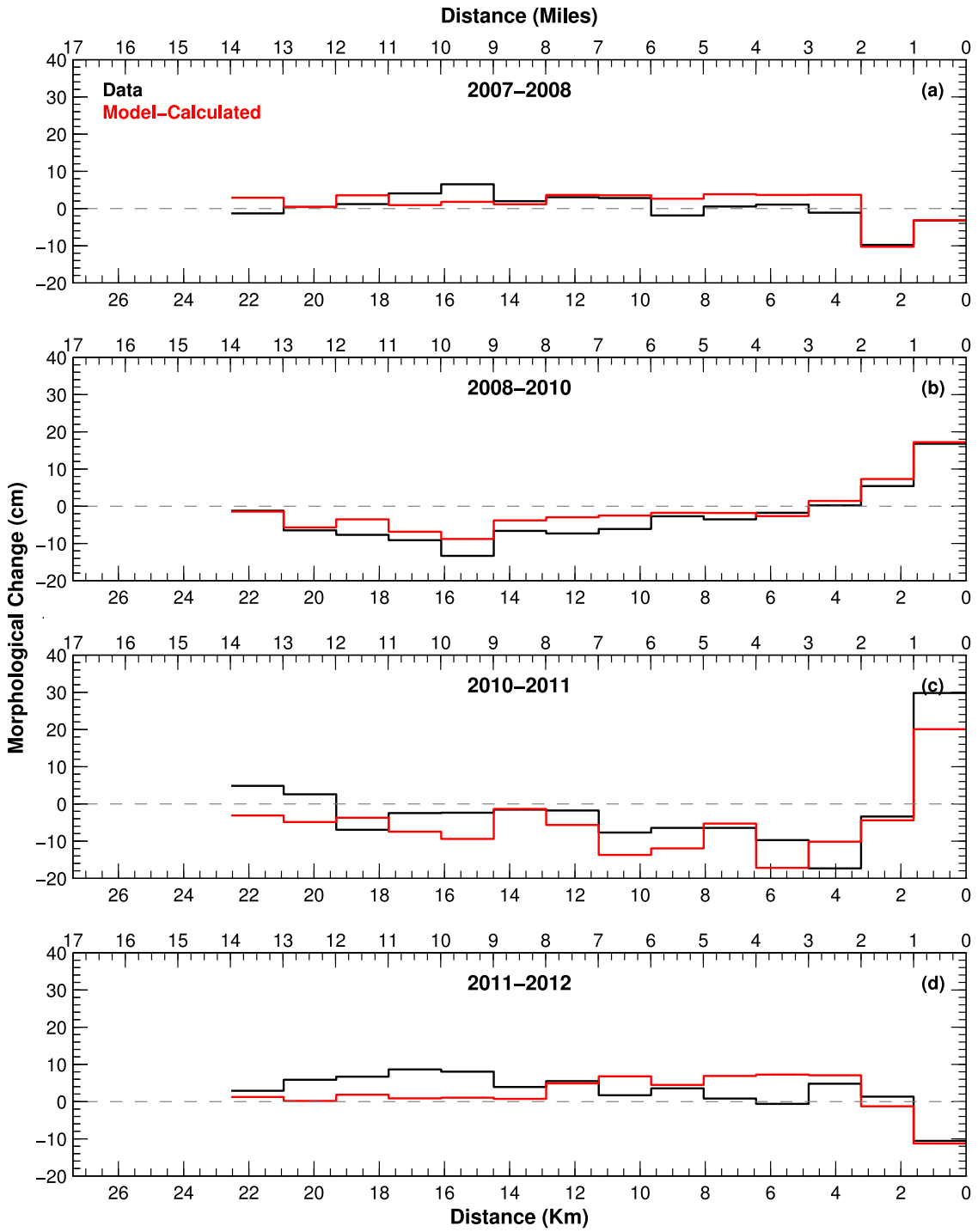

Fig. 6. Comparison of measured and model-calculated longitudinal profile of morphological change in the LPR over various survey periods laterally and longitudinally averaged over 1.6 km (1 mile) intervals. Positive values indicate net deposition and negative values indicate net erosion. Morphological change over the (a) 2007–2008, (b) 2008–2010, (c) 2010–2011, and (d) 2011–2012 survey periods.

decreasing τ_{Cr}, and decreasing erosion rate (for given shear stress) with depth in the bed. The consolidation model also allows for the instantaneous profile of these metrics to deviate from the equilibrium profile as a function of the time history of erosion and deposition, and eventually tending to the equilibrium profile. In other words, a less-erodible layer exposed by erosion will swell and become more erodible over time, a temporal trend that is conceptually reasonable and relevant for long-term morphological simulations in dynamic settings. Furthermore, the depth- and time-dependent erodibility parameterized in the bed layering (via the fluff and transition layers, and the consolidation model) allows for representation of memory effects, sediment mobility, and the various time-scales responsible for morphological evolution in fine sediment systems. This is a key aspect of the modification to the classical morphodynamic loop presented in Fig. 4.

It should be noted that only bed layers comprised of predominantly fine sediments (fines fraction >15%; (Winterwerp and van Kesteren, 2004)) are treated as cohesive and subject to consolidation, with erosion defined using Eq. (3) through (5). Bed layers comprised predominantly of sand (fines fraction <15%) are not considered to be cohesive, i.e., they do not consolidate and have τ_{Cr} that is independent of layer density.

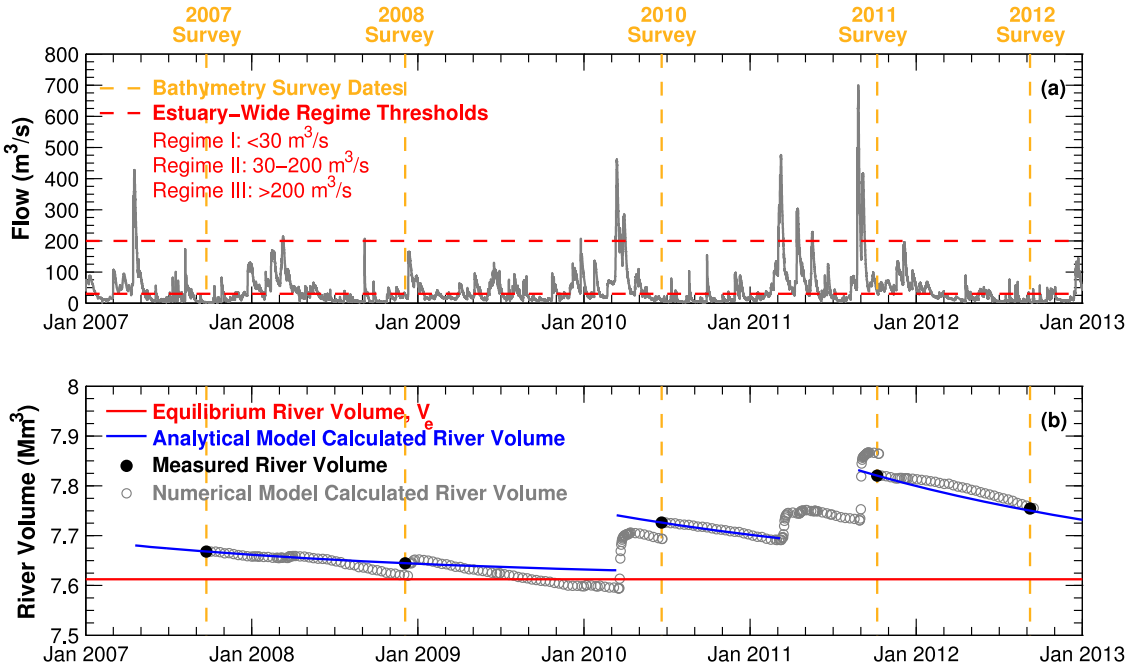

Fig. 7. Time-series of measured flow rate at the head-of-tide in the LPR over the period of the bathymetry surveys, and comparison of measured and model-calculated (analytical and numerical) river volume (at mean sea level).

Erosion properties (coefficients A and n in Eq. (5)) for such non-cohesive layers was defined using Sedflume experiments on quartz particles (Roberts et al., 1998), with erosion rates calculated using a simplified version of Eq. (5) that does not include the dependency with density. The model includes six particle classes, of which three are sand-sized (effective diameters 150 μm, 750 μm, and 4000 μm; calculated using grain size distribution measured in sediment cores), and three are fine sediment classes representing fines originating from freshwater sources (head-of-tide), from marine sources (Arthur Kill and Kill van Kull), and from the bed by erosion. Although flocculation is not modeled explicitly, the impact of flocculation is parameterized in the model as discussed in the following paragraph. The two larger sand fractions are found in only a small portion of the LPR, predominantly towards its head, with significant loadings of fine sand entering the LPR only during episodic events. Class-specific τ_{Cr} was defined for sands using the Shields curve (van Rijn, 1993), with erosion of sands from cohesive layers occurring only when both the class-specific and density-dependent τ_{Cr} is exceeded. In contrast, erosion of sands from non-cohesive layers occurs when the class-specific τ_{Cr} is exceeded.

Initial conditions corresponding to the mass fractions of the various classes in the sediment bed (fines in bed at initialization were assigned to the bed fines class) and dry density were defined using measurements on sediment cores from the LPR (Moffatt Nichol and Deltares, 2019) and assigned as averages over large reaches. The fluff and transition layers were also initialized at their maximum allowable thickness. Temporally varying SSC boundary conditions were defined at the head-of-tide (varying in response to river flow), and at the marine boundaries (varying within the tidal cycle as a function of tidal currents) using rating curves (Moffatt Nichol and Deltares, 2019). The settling velocities of the sand classes were determined using the formulation of Cheng (1997). The settling velocity of fines originating from the head-of-tide was calculated using Cheng (1997) on the basis of an effective diameter measured with laser diffraction on deflocculated suspended sediment samples (Moffatt Nichol and Deltares, 2019). Effectively, this assumes that fines originating from the freshwater sources are poorly flocculated, an assumption verified during model performance assessment. In contrast, the settling velocities of fines originating from marine sources and from the bed were developed by calibration to SSC/SSF and morphological change data; these correspond to higher values than the fines from the head-of-tide, likely reflecting the effect of floc formation in the water column and in the bed (Winterwerp, 2002, Tran and Strom, 2019). Furthermore, in an approximation of aggregation processes in the bed (Tran and Strom, 2019), fines from freshwater and marine sources that accumulate underneath the fluff and transition layers (i.e., implicitly have been residing in the bed for one or more tidal cycles) are instantaneously transferred to the bed fines class. Probability of deposition for the sand classes is defined using Gessler (1967) whereas probability of deposition for the fines is set to 1 (i.e., allowing deposition under all conditions; see Winterwerp and van Kesteren (2004)). Table 1 provides a tabulation of the major model parameter values.

Finally, the effect of shipping at locations seaward of RM 2 was parameterized for simulations spanning the 2007-2008 and 2011-2012 bathymetry surveys by using the measured morphological change over these periods. Up to five ships on average transit this reach on a daily basis (Moffatt Nichol and Deltares, 2019), with the scour expected to be related to factors such as the timing of transit related to the tide, vessel draft, power applied by the propellers at any given location, etc. However, given data limitations, such subtleties are ignored, and the measured erosion was used to specify a constant rate of erosion at the locations of observed scour, and the scoured mass assigned as a continuous and vertically-uniform loading to the water column

3.2. *Model performance*

Model performance was evaluated by comparison against measurements for various metrics over a range of river flows and time periods. Model-data comparisons for small- and large-scale morphological change are presented here; Appendix A presents comparisons for currents, salinity, SSC, SSF, and cumulative morphological change along with a discussion of model limitations.

Model performance was compared to the measured morphological change over 2007–2012. The morphodynamic model was used to perform four separate simulations spanning the periods of the various bathymetry surveys, and initialized using measured bathymetry at the start of the particular period. The measured and calculated morphological changes were averaged cross-sectionally and longitudinally over

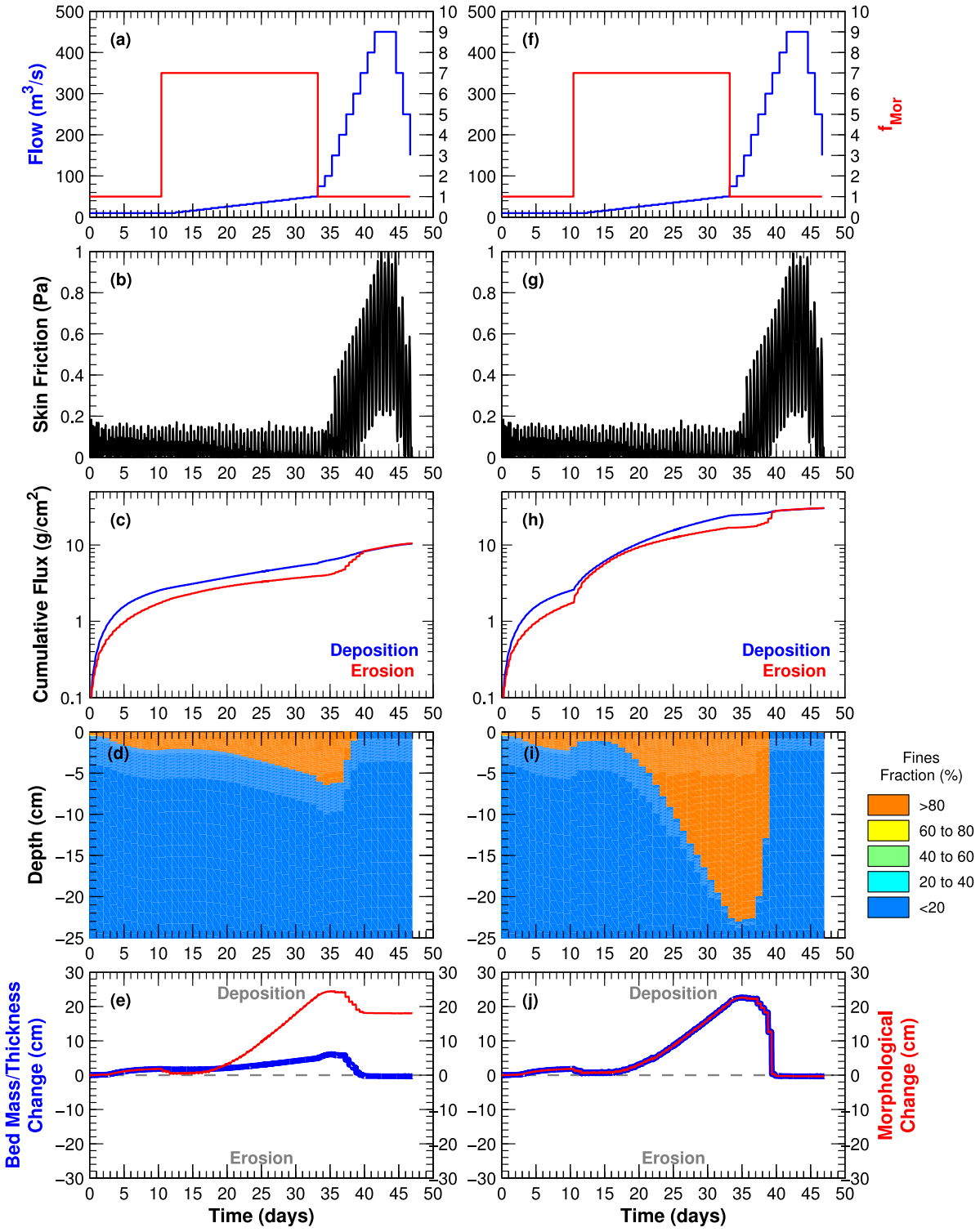

Fig. 8. Comparison of model performance over a synthesized hydrograph with morphological upscaling applied to bed level changes (panels a through e), and with morphological upscaling applied to bed mass changes (panels f through j).

1 mile (1.6 Km) intervals for an assessment of large-scale morphological changes and are shown in Fig. 6. Overall, the model reproduces the large-scale flow-dependent morphological trends apparent in the data – results for the low-flow periods (2007–2008 and 2011–2012) generally show infilling landward of RM 2, and the high-flow periods (2008–2010 and 2010–2011) show erosion landward of RM 2 and deposition seaward of RM 2. In the model, erosion scales with river flow rate – for instance, the 2008–2010 period included a 450 m^3/s event whereas the 2010–2011 period included a 700 m^3/s event, and accordingly, the model responds with more erosion during the latter period. The data show such flow-dependent erosion depths in some reaches, e.g., between RM 2 and RM 6. However, in other reaches, specifically between RM 7 and RM 11, while the data shows evidence of armoring during the 2010–2011 period, the model does not capture the armoring effects. Although the model reproduces the large-scale flow-dependent erosional and depositional trends, and the large-scale morphological

changes, it tends to under-perform at local scales.

The model-calculated river volume in the simulations covering the 2007–2012 period was also compared to the measured river volume as shown in Fig. 7. In addition, the measured infill landward of RM 2 during the low-flow years was examined analytically for an assessment of large-scale morphodynamics using the Volume-of-Cut method (Winterwerp et al., 2021) which describes the infill rate as $\frac{dV}{dt} = \frac{V-V_e}{T}$, with solution:

$$V_t = V_e + (V_0 - V_e)\exp\left(-\frac{t}{T}\right) \tag{6}$$

where, T is the time-constant for the infill process, and V is the cumulative submerged river volume (calculated at MSL) landward of RM 2, with subscripts t, e, and 0 representing instantaneous, equilibrium, and initial quantities. Eq. (6) was used to describe the infill process between the 2007–2008 and 2011–2012 surveys using the measured initial (V_0) and final (V_t) river volumes, and the two unknowns, V_e and T, calculated as 7.61 Mm^3 and 823 days, respectively, using least-squares optimization. The resulting trends in analytical model estimates of river volume shown in Fig. 7 are, with some exceptions, generally consistent with the results of the numerical model.

Fig. 7 also shows that the measured river volumes in 2007 and 2011 were only 0.7% and 2.7% greater, respectively, relative to V_e, and the measured river volumes in all five surveys is very similar to V_e. This indicates that, as a whole, the reach landward of RM 2 is at or near morphodynamic equilibrium, with episodic Regime III events causing only a relatively small deviation from equilibrium. This suggests possible explanations for the under-performance of the model with respect to small-scale spatial erosion and infill patterns. Specifically, scour in erosion-limited conditions is very sensitive to local variations in bed stratigraphy, both with respect to the armoring effects of sand lenses as well as low-erodibility, consolidated layers. Model results are therefore limited by the lack of comprehensive data characterizing such spatially- and depth-varying properties. Similarly, because the change in river volume by erosion is not significant enough to significantly enhance trapping efficiency in the following periods, local patterns of infill are expected to be more sensitive to the availability of sediment at the mouth of the LPR and its synchronization with import mechanisms, especially in the case of shipping-induced scour. For instance, in locations where navigation is limited by water depth, ship traffic may be limited to the period of the rising or flood tide, which implies greater potential for sediment import into the LPR than if the scour is distributed equally over the entire tidal cycle as assumed in the numerical model. However, such limitations may impact model performance more over the short-term such as the inter-annual periods presented here than over the long-term (Dam et al., 2016). Therefore, the application of the Morfac approach to the LPR presented in the next section also includes a validation of model performance over a multi-decadal period.

4. Morphodynamic upscaling using morphological acceleration

The morphodynamic model of the LPR was used in the development and application of the Morfac approach for fine sediment settings. The Morfac approach derives from the following key concepts (Lesser et al., 2004, Roelvink, 2006, Ranasinghe et al., 2011, Lesser, 2009):

- Time-scales of morphological change are typically greater than time-scales of change in hydrodynamic forcings.
- Morphological change or net change in bed sediment mass (e.g., in response to a repeated sequence of identical hydrodynamic forcings) is assumed to be linear within the morphological timestep. This implies that morphological change or net change in bed sediment mass calculated over a single tidal cycle can be upscaled to n tidal cycles using the morphological acceleration factor, $f_{mor} = n$.

This gives rise to the notion of the morphological timestep, Δt_{mor}:

$$\Delta t_{mor} = f_{mor}\Delta t_{hyd} \tag{7}$$

where, Δt_{hyd} is the hydrodynamic timestep (which we implicitly assume equals the sediment transport timestep). Net change in bed sediment mass over the morphological timestep is calculated using erosion and deposition fluxes over the hydrodynamic timestep:

$$\Delta S_{mor} = f_{mor}(D - E)\ \Delta t_{hyd} \tag{8}$$

where, ΔS_{mor} is the mass change in the bed over the morphological timestep. In the LPR, where the river flow regime is the primary determinant of sediment dynamics (see Fig. A.3, and Mathew and Winterwerp 2020), morphological acceleration is achieved by upscaling the morphological response to given river flow rate. In other words, the net change in sediment mass in the bed associated with a given river flow that repeats over n tidal cycles is calculated by simulating a single tidal cycle for that river flow and scaling the resulting bed mass change to n tidal cycles using Eq. (8).

Note that although some authors have applied Eq. (8) (i.e., morphological upscaling applied to bed mass change; (Frings and Ottevanger, 2011)), the classical approach to morphodynamic upscaling using the Morfac approach consists of multiplying bed level changes with f_{mor} to calculate bathymetry at the end of the morphological timestep (Roelvink, 2006; Ranasinghe et al., 2011) as shown in the left panel of Fig. 4. The classical approach was tested initially as part of the current research. Briefly, in this approach, bed level change calculated over the hydrodynamic timestep (Δh_{hyd}) is multiplied by f_{mor} to calculate the bed level change over the morphodynamic timestep (Δh_{mor}); see Eq. (9).

$$\Delta h_{mor} = f_{mor}\Delta h_{hyd} \tag{9}$$

Application of Eq. (9) to perform morphological upscaling in the numerical model implies that morphological change will not be consistent with sediment mass change in the bed. In contrast, Eq. (8) results in bed mass change that is consistent with morphological change and allows for appropriate representation of memory effects and sediment mobility. This is illustrated with an application of the two morphodynamic upscaling methods to a synthesized hydrograph in Fig. 8.

The example application in Fig. 8 uses the same model application presented in the preceding section and includes a synthesized hydrograph starting at below-average river flow of 10 m^3/s and increasing to 450 m^3/s. The first 10 days of this simulation represent the hydrodynamic and sediment transport spin-up and is simulated using f_{mor} of 1. Subsequently, f_{mor} increases to 7 as flow increases to 50 m^3/s, at which point f_{mor} decreases to 1. The model was initialized with a bed comprised of the fluff and transition layers, and sub-surface layers comprised solely of the largest sand class included in the present application (which has $\tau_{Cr} = 3.1$ Pa and is non-erodible under the shear stresses imposed in this example). Model performance is shown on the left panels using the classical approach to morphodynamic upscaling (Eq. (9)), and on the right panels using the approach used in this paper (Eq. (8)) for a grid cell located at RM 1.4 in the LPR.

Review of model performance for bed composition (panels d and i) and bed mass/thickness and morphological change (panels e and j) shows the artifact associated with the classical morphodynamic upscaling approach in a setting affected by bed armoring. The first 37 days of the simulation represent net depositional conditions, with both simulations showing net morphological change of approximately 24 cm. Since the classical approach does not preserve bed mass, the change in bed mass/thickness is only about 6 cm and much lower than morphological change during this period. This is also seen in the bed composition change over time, with the depositing fines creating about 6 cm of new layers on top of the initial bed layers. In contrast, the simulation with morphodynamic upscaling applied to bed mass preserves bed mass change and morphological change, with the depositing fines creating

about 24 cm of new layers on top of the initial bed layers. During the high shear stress conditions over days 37–40, the entire depth of newly deposited sediment is eroded because skin friction during this period exceeds the critical shear stress of the deposited fine sediment layers. In the case of the simulation with morphodynamic upscaling applied to bed mass change, net erosion during this period is about 24 cm, with bathymetry reverting to the initial bathymetry following exposure of the armored bed layers. However, in the simulation with morphodynamic upscaling applied to bed level change, erosion of the 6 cm of deposited fines exposes the armored bed layer, and consequently, net morphological change over the 47-day simulation is calculated as net accretion (about 18 cm more deposition than the simulation with morphodynamic upscaling applied to bed mass change). This artifact in performance is a consequence of the fact that the classical approach does not properly account for the factors leading to memory effects in the bed. The same artifact is also introduced for a purely fine sediment setting, where memory effects due to depth-dependent erodibility can have a similar effect as armoring in this example. The analysis indicates that the classical approach is appropriate only in settings where erosion-limited transport is not a factor, e.g., typically, problems of sand transport in coastal settings. Morphodynamic upscaling in settings where memory effects are relevant for transport can be successfully achieved only by applying upscaling to the bed mass change.

The Morfac approach involves input reduction for the hydrodynamic forcings, which in the case of the LPR includes river flow and barotropic forcing. Briefly, input reduction for the barotropic forcing seeks *to replace the complex time series of tidal water level and current fluctuations occurring in nature with a simplified tide that produces the same residual sediment transport and morphological change patterns as the naturally varying tides* (Lesser, 2009). In the case of fine sediment systems, the representative tide should also reproduce the effects of sediment availability and erosion-limited transport on residual sediment transport. The representative tide used for boundary conditions in the application of the Morfac approach include the semi-diurnal M_2 and diurnal O_1 and K_1 constituents along with the M_4 and M_6 overtides, with the representative tide (tidal range of 1.5 m) synthesized following the methods of Lesser, 2009). Simulations using the representative tide were compared to simulations using the spring-neap tidal cycle in order to ensure that the representative tide preserves the long-term net sediment transport. SSC boundary conditions at the marine boundaries were specified using the rating curve approach described previously and using tidal currents corresponding to the representative tide. Input reduction for river flow is discussed in the following section.

4.1. Considerations for Morfac approach in fine sediment settings and specifically for application to the LPR

Section 1 includes discussion of phenomena specific to fine sediment transport. Specific formulations and careful selection of model inputs were required for appropriate representation of these phenomena within the context of the Morfac approach. These considerations maintain the assumption of linearity within the morphological timestep that is key to the Morfac approach, separate conditions when the assumption of linearity cannot be met, and preserve the various time-scales of morphological response in fine sediment systems. These are summarized below:

- Residual sediment transport – Morphological change due to residual transport associated with barotropic and baroclinic circulation (relevant during Regimes I and II) scales as a function of time. For instance, a sediment particle located at the mouth of the river at the start of a flood tide will move a certain distance up-estuary after one tidal cycle due to tidal asymmetries and lag effects (assuming flood dominance), and estuarine circulation. During the following tidal cycle, it will move some distance further up-estuary. In other words, net sediment transport in a simulation of two tidal cycles with $f_{mor} = 1$ will not be identical to a simulation of one tidal cycle with $f_{mor} = 2$. This implies a practical upper-bound on the value of f_{mor}, established by trial-and-error as 7 and applicable during Regimes I and II in the current application.
- Memory effects – Consider a time-series of two identical erosional events occurring sequentially and in short order. High shear stress during the first event can cause erosion of surficial sediments, thus exposing a bed layer with τ_{Cr} greater than the maximum bed shear stress during the event. Therefore, the second event, which experiences the same time-history and magnitude of bed shear stress as the first event, would not be expected to cause any further erosion. However, a simulation of a single event with $f_{mor} = 2$ will overestimate the magnitude of erosion compared to a simulation of two sequential events with $f_{mor} = 1$; the latter will preserve the erosion-limited morphological response. In the LPR, depth-dependent erodibility is a factor in limiting erosion primarily under Regime III conditions (river flow rate greater than 200 m^3/s for the system as whole, although this threshold decreases in the landward direction). Therefore, in order to appropriately represent such memory effects, for the current application, morphological acceleration is not employed (i.e., $f_{mor} = 1$) when river flow rate exceeds 50 m^3/s which is a threshold established using maps of bed shear stress under different steady-state river flow rates and is the estimated threshold above which erosion of the consolidated layers may occur (Mathew and Winterwerp, 2020).
- Supply-limited transport – The supply of fine sediments from the head-of-tide generally tends to be event-dominated, i.e., episodic high-flow events are responsible for a significant fraction of the annual sediment delivery to the river and affect sediment availability for redistribution during subsequent periods. Morphological acceleration under such conditions may not accurately reproduce sediment transport patterns. For instance, for a high-flow event loading with a travel time of 10 days from the head-of-tide to the area of interest, a one-day simulation with $f_{mor} = 10$ will not capture transport to the area of interest. Therefore, in order to appropriately represent such supply-limited transport, for the current application, morphological acceleration is not employed (i.e., $f_{mor} = 1$) when river flow rate exceeds 50 m^3/s. This threshold is also consistent with the rating curve used to define SSC boundary conditions at the head-of-tide which includes relatively constant SSC at river flow rate of less than 60 m^3/s and increasing with increasing river flow.
- Fluff layer dynamics – In order to preserve the intra-tidal SSC and SSF dynamics, which depend on sediment inventory in the fluff layer and is relevant for residual transport, only the sediment flux over the hydrodynamic timestep, i.e., $(D - E)\Delta t_{hyd}$, is added to or sourced from the fluff layer. Sediment flux over the remainder of the morphological timestep, i.e., $(f_{mor} - 1)(D - E)\Delta t_{hyd}$, is added to or sourced from subsurface layers. This preserves the timing of erosion (and deposition) within the tidal cycle, thus preserving residual transport over the tidal cycle, and is important for maintaining the condition of linearity in morphological change during the morphological timestep that is key to morphological upscaling.

These considerations have resulted an approach that includes river flow-dependent values of f_{mor}, with f_{mor} of 7 or 1 when river flow rate is less than or greater than 50 m^3/s, i.e., Regime I/II or Regime II/III conditions, respectively. The selected river flow threshold separates conditions where erosion is limited to the fluff layer (river flows < 50 m^3/s) from conditions where the consolidated layers underneath the fluff layer may be eroded. This definition of conditions without morphological acceleration preserves erosion-limited dynamics and preserves supply-limited transport which are relevant during high river flows. Furthermore, the selected f_{mor} value of 7 in combination with the formulation described previously that preserves fluff layer dynamics, helps preserve residual sediment transport which is a key driver of morphological change during Regimes I/II.

Table 2
Quantitative performance assessment of model simulations using the Morfac approach compared to the brute force simulations for various combinations of f_{Mor} and the flow threshold separating the conditions with variable values of f_{Mor}.

Morfac Approach – Simulation Scenario			Simulation Performance – Brier Skill Score			
Regime I & II f_{Mor}	Regime II & III f_{Mor}	Flow Threshold (m^3/s)	2007–2008	2008–2010	2010–2011	2011–2012
1	1	-	0.96	0.92	0.93	0.96
3	1	50	0.96	0.92	0.91	0.94
5	1	50	0.96	0.92	0.91	0.93
7	1	50	0.95	0.91	0.91	0.92
10	1	50	0.91	0.90	0.91	0.90
15	1	50	0.87	0.89	0.90	0.85
7	1	25	0.95	0.91	0.90	0.93
7	1	75	0.93	0.91	0.92	0.90
7	1	100	0.92	0.91	0.92	0.89
7	3	50	0.84	0.65	0.72	0.88
7	5	50	0.74	0.46	0.63	0.88

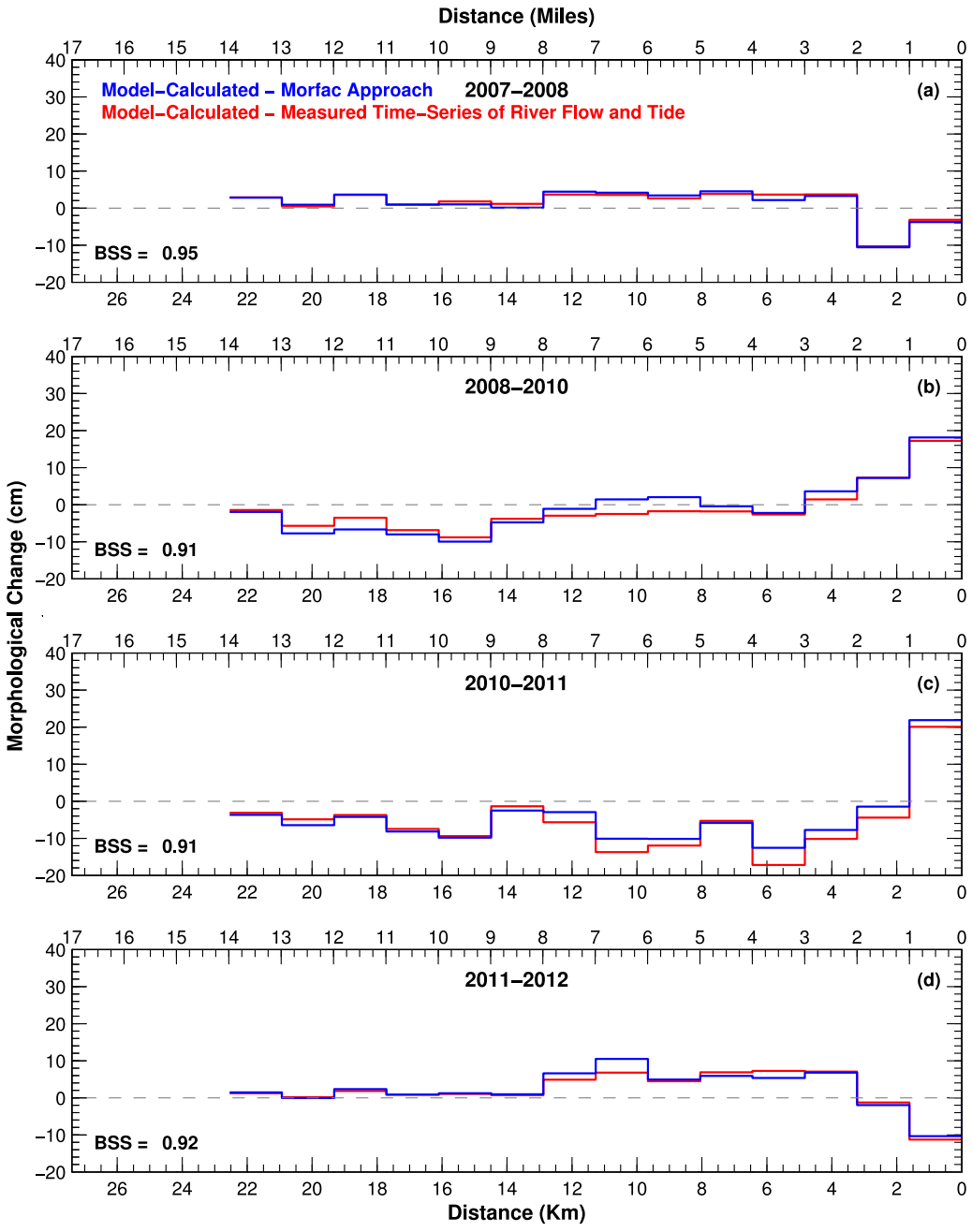

Fig. 9. Comparison of model-calculated longitudinal profile of morphological change in the LPR over various survey periods laterally and longitudinally averaged over 1.6 km (1 mile) intervals. Positive values indicate net deposition and negative values indicate net erosion. Morphological change over the (a) 2007–2008, (b) 2008–2010, (c) 2010–2011, and (d) 2011–2012 survey periods. Results for model simulations using the measured time-series of river flow and tide, and for model simulations using Morfac.

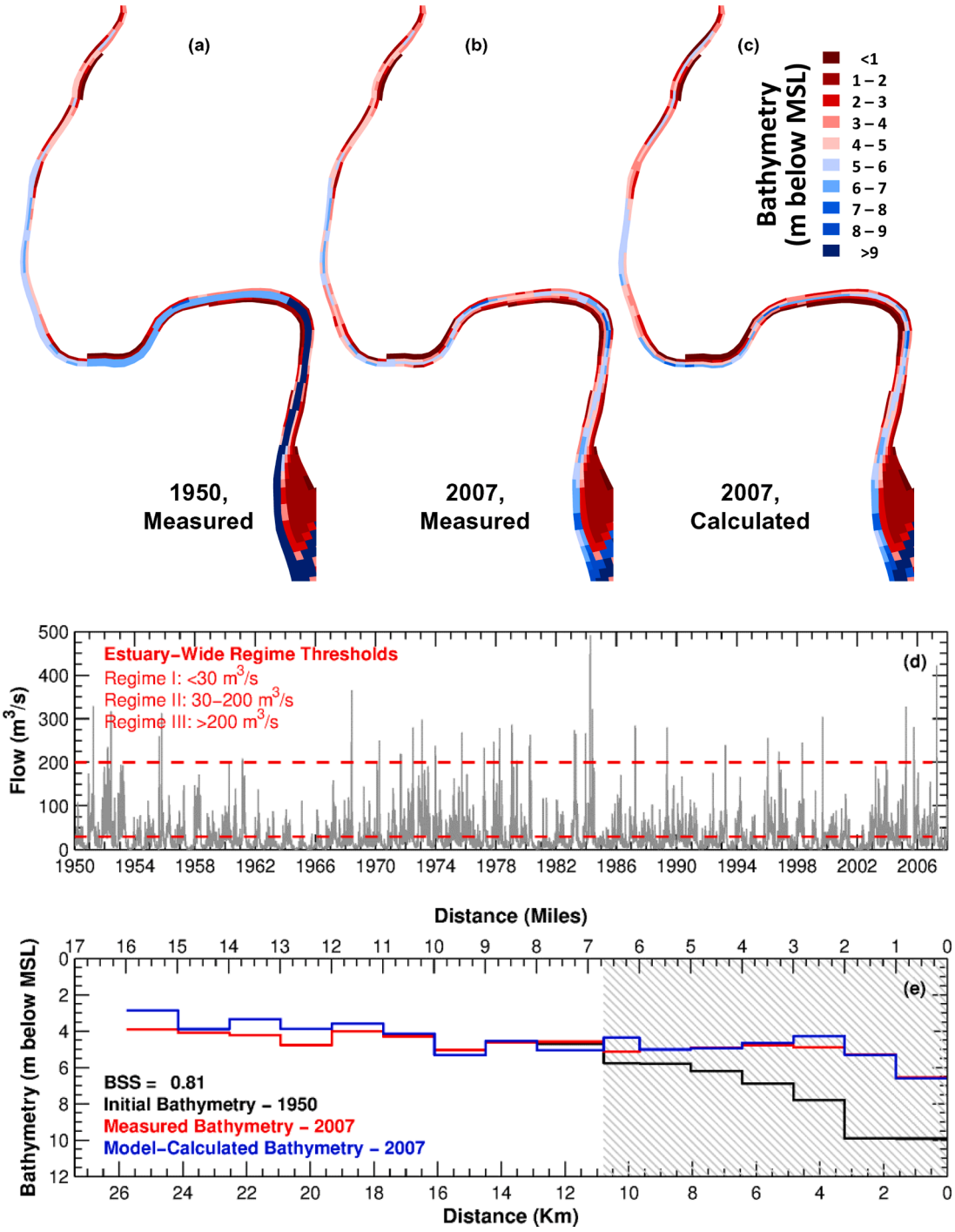

Fig. 10. Validation of morphological model using Morfac using the measured infill of the LPR between RM 0 and RM 6.7 over 1950–2007. Maps of bathymetry at various times (a–c), time-series of river flow during 1950–2007 (d), and longitudinal profiles of bathymetry (e) in the navigation channel – post-dredging in 1950–1951, measured in 2007, and model-calculated in 2007 (hatched region indicates extent of dredging in 1950–1951).

The river flow boundary conditions are a synthesized sequence of flow rates designed to represent the river flow-dependent location of the salt-front and ETM, and effects of barotropic and baroclinic circulation on net sediment transport. This was accomplished by sorting the measured river flows (averaged over the period of two tidal cycles in order to account for the inequality in the semi-diurnal representative tide), followed by a fixed-window average (over seven two-tide cycles) of river flows for flow rates less than 50 m^3/s. For simulations covering the periods of the inter-annual bathymetry surveys, this sorting and sequencing was performed separately for periods before and after significant high-flow events between two surveys, with the synthesized river flow rate increasing from the start of the simulation up to the peak of the high-flow event, followed by decreasing river flow rate. This preserves the timing of the high-flow event in a fashion analogous to the brute-force simulations. SSC boundary conditions at the head-of-tide were defined using rating curves as described previously.

4.2. *Model performance*

With the exception of the boundary conditions for tide, river flow,

and SSC (defined as described above), the remainder of the model setup and parameterization for the morphodynamic model using Morfac is identical to the setup presented in the preceding section. The performance of the morphodynamic model using Morfac is first compared against the brute-force simulations over the period of the inter-annual bathymetry surveys (2007–2012). This serves as test of the Morfac approach in its ability to reproduce the results of the more computationally intensive approach. Subsequently, as a validation, the morphodynamic model using Morfac is applied for a multi-decadal hindcast simulation and compared against measured morphological change.

4.2.1. Model tests – 2007–2012

The value of f_{mor} used for periods simulated with morphological acceleration and the flow threshold used to separate periods with and without morphological acceleration were developed based on the results of morphological change in test simulations covering the period of the inter-annual bathymetry surveys over 2007–2012. Table 2 presents a quantitative model performance assessment for various parameter values for f_{mor} and the threshold river flow. The performance of the individual test simulations was assessed against the results of the brute-force simulations (using model results in individual grid cells) using the Brier-Skill Score (BSS) as defined by van Rijn et al. (2003) and Sutherland et al. (2004):

$$BSS = 1 - \frac{\langle (Y - X)^2 \rangle}{\langle (B - X)^2 \rangle} \tag{10}$$

where, X can be the measured bed level or calculated bed level from brute force simulations, Y is the model-calculated bed level in simulations using the Morfac approach, B is the initial bed level, and the angled brackets denote an arithmetic mean. For the assessment in this section, X is the calculated bed level from the brute force simulations (results presented in Fig. 6) and the BSS is used to assess how well the simulations using morphological acceleration reproduce the brute-force simulation results. A BSS of 1 indicates a perfect match whereas decreasing value of BSS indicates increasing divergence between the two sets of model results.

The results in Table 2 show progressively worsening results with (1) increasing value of f_{mor} for the periods with morphological acceleration (during Regime I & II flows), (2) morphological acceleration during Regimes II and III, and (3) increasing flow threshold used to separate periods with and without morphological acceleration. These comparisons were used to determine selection of $f_{mor} = 7$ for periods simulated with morphological acceleration and the flow threshold of 50 m^3/s. In addition, the results for the simulation without morphological acceleration (i.e., $f_{mor} = 1$ during all flows) also shows the impact of the representative tide and the synthesized flow sequencing applied as part of the Morfac approach – overall, these simplifications of the boundary conditions do not significantly impact the results for morphological change, i.e., the accuracy of the predictions.

Fig. 9 shows comparisons of model results for the brute-force simulations, and for simulations using Morfac (using $f_{mor} = 7$ for periods with morphological acceleration and flow threshold of 50 m^3/s). Both graphical as well as quantitative comparisons indicate a high degree of similarity between the two sets of model results. Minor differences apparent in the comparisons are primarily related to factors not included in the simulations using Morfac, e.g., coincident spring tide during some of the high-flow events, impact of stochastic variations in river flow on residual sediment transport, etc. Nonetheless, overall, the simulations using Morfac reproduce the large-scale as well as local-scale (with some minor exceptions) performance of the brute-force simulations. Therefore, the morphodynamic model using Morfac is concluded to be reasonably similar to the more computationally intensive approach, and subject to the validation presented in the following sub-section, a valid approach for computationally efficient morphological simulations in fine sediment settings.

4.2.2. Model validation – 1950–2007

The hindcast simulation used to validate the long-term performance of the morphodynamic model using Morfac involves the historical infill of the navigation channel in the LPR. The last major dredging in the LPR occurred in 1950–1951 between RM 0 to RM 2.2, RM 2.2 to RM 4.2, and RM 4.2 to RM 6.7, to depths of 9.9 m, 6.8 m, and 5.6 m, respectively (depths relative to MSL), with maintenance dredging (to depth of 9.9 m) between RM 0 and RM 1.5 in 1983 (U.S. Army Corps of Engineers, 2010). Fig. 3 also includes the cross-section in 1950-1951 for comparison to the 2007 configuration – significant deviations from the near-equilibrium conditions in 2007 are apparent, especially between RM 2 and RM 5. Subsequent infill of the navigation channel ranges up to about 5 m in some locations. Therefore, the morphodynamic model using Morfac was applied for a simulation over the period 1950-2007 with the bathymetry in the navigation channel between RM 0 to RM 6.7 initialized at the design dredge depths, and bathymetry between RM 0 to RM 1.5 reset to the design dredge depths in 1983. Periodic changes in the geometry and morphology within Newark Bay (U.S. Army Corps of Engineers, 2006) were also represented in the simulation. Input reduction for river flow at the head-of-tide was performed in annual cycles using the historic river flow data from 1950-2007. The impact of navigation in the channel between RM 0 and RM 2 was included by constraining deposition as a depth-limited process in this reach, with the limiting depth being the measured bathymetry in 2007. Fig. 10 shows the hydrograph during this period; key observations include the extended period from the mid-1950s to late-1960s when river flow was relatively low (mostly Regime I, i.e., infilling), with only one Regime III event. In contrast, the remainder of this 58-year period experienced thirty-two Regime III events.

Fig. 10 shows a comparison of the measured and model-calculated bathymetry in 2007. Overall, the model reproduces various spatial and temporal trends apparent in the data. These include the magnitude of infill at local scales, trend of decreasing infill with distance in the landward direction, and relatively lower infill in the vicinity of bends in the river. Quantitative assessment of the model-calculated and measured bathymetry in 2007 shows BSS value of 0.81 which represents an "excellent" model performance accordingly to the performance classification scheme of van Rijn et al. (2003); Eq. (10) was used to calculate BSS with X representing the measured bed level in 2007. Therefore, this validation using multi-decadal data provides demonstration of the applicability of the Morfac approach for performing long-term morphological simulations in fine sediment settings.

5. Model application

The morphodynamic model using Morfac was applied to answer a few specific and general questions regarding the current morphological status of the LPR and the morphological impact of specific forcings. The specific question pertains to the impact of navigation seaward of RM 2, and the general questions pertain to the current morphological status of the LPR landward of RM 2, the role of episodic Regime III events, and the impact of climate change. The prognostic simulations used to address these issues were initialized using the measured bathymetry in 2007. The hydrograph over 1950–2007 is representative of the long-term measured river flow (over 1897–2020). Therefore, except as described later in the context of episodic Regime III events and climate change, the prognostic simulations use the river flow hydrograph from 1950 to 2007. In addition, the simulated 58-year duration is much larger than the approximately 2-year infill time-scale estimated using the Volume-of-Cut method, implying that the simulated duration is adequate for assessing questions related to morphological equilibrium of the system. These simulations do not include shipping-induced scour in the LPR.

5.1. Role of navigation and current morphological status

Several lines of evidence indicate that the reach between RM 0 and

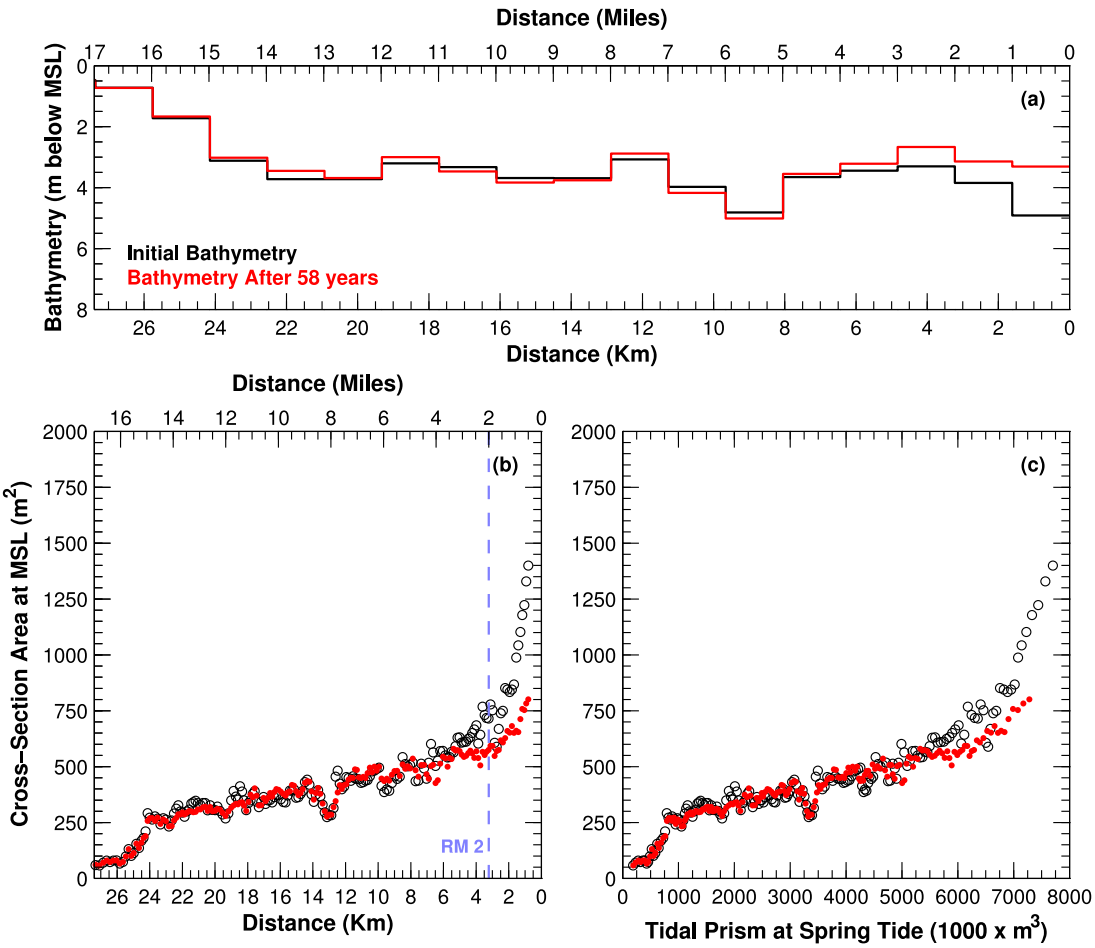

Fig. 11. Application of the morphodynamic model using Morfac to assess the impact of navigation between RM 0 and RM 2 in the LPR. Longitudinal profiles of bathymetry (a) and cross-sectional area (b), and tidal prism to cross-section relationship (c) – measured in 2007, and model-calculated after a 58-year prognostic simulation.

RM 2 in the LPR is impacted by shipping activities:

- a change in the trend of current river cross-section area with distance and with tidal prism at RM 2 as presented in Fig. 3,
- erosional trends between RM 0 to RM 2 during the low-flow periods (2007–2008 and 2011–2012) in the inter-annual morphological changes as presented in Fig. 2, and the consideration that the erosion cannot be caused by natural hydrodynamic forcings – model-calculated bed shear stresses during the periods of erosion are not high enough to cause the noted magnitude of erosion, and
- local-scale spatial patterns of erosion that are consistent with marine traffic data (Moffatt Nichol and Deltares, 2019).

Collectively, these lines of evidence indicate that this reach of the LPR is impacted by ongoing shipping activities. Therefore, the impact of navigation was assessed using a prognostic simulation that does not include shipping-induced scour. Fig. 11 shows the resulting comparison of initial and calculated bathymetry at the end of the simulation, and the cross-section area and its relationship with tidal prism using the initial and final model-calculated bathymetry. The comparisons indicate that the reach between RM 0 and RM 2 which currently experiences shipping-induced scour, will infill by up to 2-3 m in some areas in the absence of navigation. The infilling sediment is a combination of sediment scoured from landward locations during Regime III events as well as sediments transported from Newark Bay by the tide and estuarine circulation. Consequently, the cross-section adapts, and seaward of RM 2, both the longitudinal profile of cross-section area and the trend of cross-section area with tidal prism tend towards a continuation of trends measured in 2007 at more landward locations. These results are consistent with the hypothesis that this reach of the LPR is currently in a state of dynamic morphological equilibrium with the ongoing shipping activities. In the absence of navigation, substantial infill will occur, reaching an equilibrium cross-section that is similar to that expected based on morphodynamic relationships apparent in more landward reaches.

Furthermore, using the river morphology at the end of the prognostic simulation, the convergence length L_A and exponent $\propto$ of 26.6 km and 0.42, respectively, are only marginally different from values based on the current morphology (presented in Section 2). These results indicate that the reach landward of RM 2 is largely at morphodynamic equilibrium, which consistent with the results of the analytical Volume-of-Cut method.

5.2. *Impact of Regime III events*

Episodic events causing significant erosion and export of sediments are considered to be the mechanism responsible for maintaining the long-term morphological equilibrium in an estuary, which may otherwise experience infilling due to import of sediments from both landward and seaward directions (Geyer et al., 2001, Meade, 1969). In the context of the LPR, Regime III events are considered to be representative of such erosional and exporting conditions (Mathew and Winterwerp, 2020). Therefore, in order to assess the significance of Regime III events on long-term morphological behavior, the results of a prognostic simulation

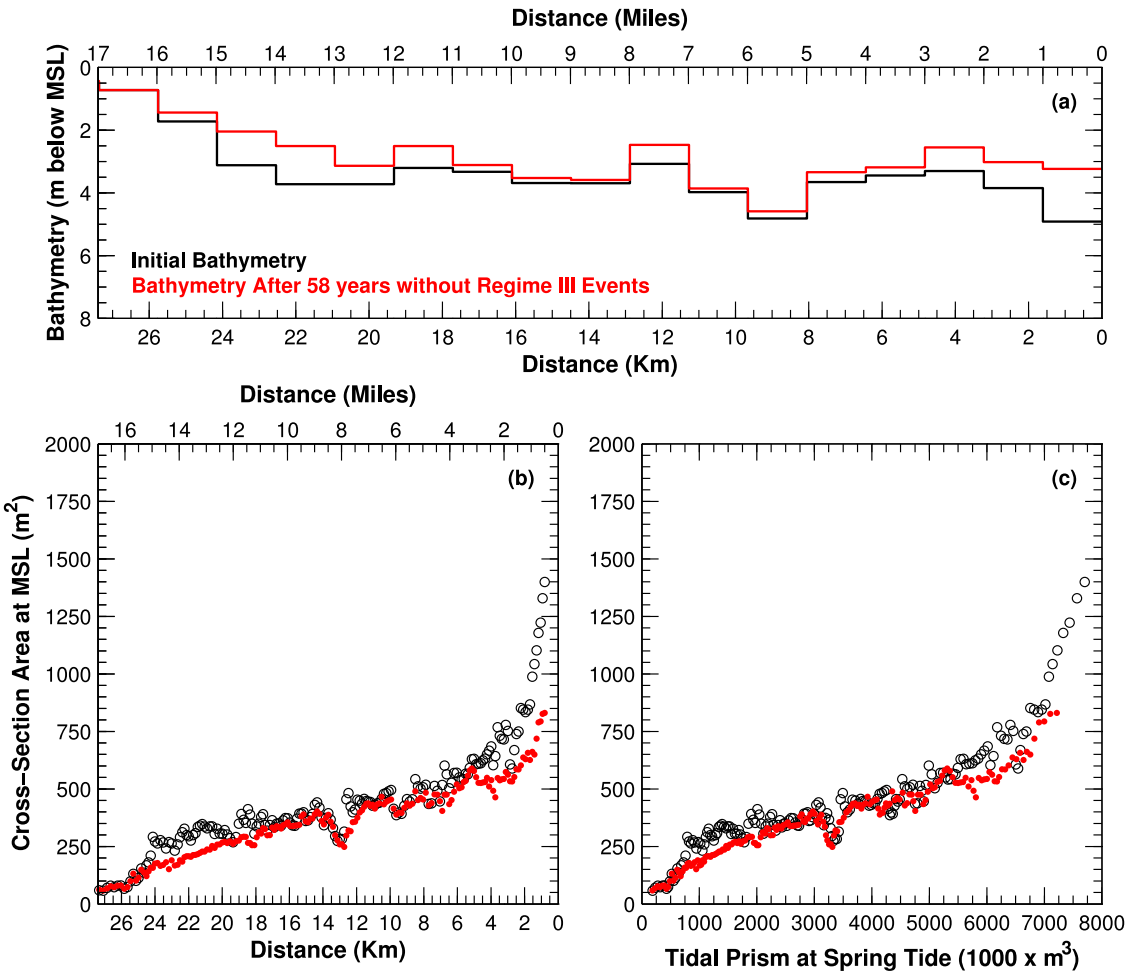

Fig. 12. Application of the morphodynamic model using Morfac to assess the impact of episodic Regime III events. Longitudinal profiles of bathymetry (a) and cross-sectional area (b), and tidal prism to cross-section relationship (c) – measured in 2007, and model-calculated after a 58-year prognostic simulation without Regime III events.

using the measured river flow hydrograph were compared to a simulation where river flow was capped at 100 m^3/s, which is the local threshold for Regime III events for the reach landward of RM 8 (Mathew and Winterwerp, 2020).

Fig. 12 shows the resulting comparison of initial and calculated bathymetry at the end of the simulation, and the cross-section area and its relationship with tidal prism using the initial and final model-calculated bathymetry. Similar to the results presented in Fig. 11 (which includes the impact of Regime III events), the results in Fig. 12 show significant infilling in the reach seaward of RM 2. However, in contrast to the results in Fig. 11, the results in Fig. 12 show infilling throughout the length of the estuary, and most markedly in the upper reaches (between RM 15 and RM 11). These results indicate a different equilibrium morphology in the absence of Regime III events, with a shallower equilibrium bathymetry than in the presence of Regime III events. These results tend to confirm the hypothesis of Geyer et al. (2001) and Meade (1969), and the empirical observations of Mathew and Winterwerp (2020) on the role of Regime III events in the long-term morphological equilibrium of estuaries. This implies such Regime III events are critical in shaping the equilibrium morphology and should be included in morphological studies of such systems.

Regime III events also impact the morphodynamic relations of cross-section profile and relationship with tidal prism. In contrast with the values for the current morphology presented in Section 2, the results in Fig. 12 show that in the absence of Regime III events, the convergence length L_A and exponent $\propto$, decrease to 19.1 km, and increase to 0.58, respectively. The decrease in convergence length is consistent with the findings of Dronkers, (2017) who showed convergence length to be a positive function of river flow velocity. Accordingly, a decrease in river flow rate (e.g., due to the lack of Regime III events), would result in a decrease in the convergence length which is consistent with the numerical model results. The decrease in cross-section area in the upper reaches also leads to the increase in the value of $\propto$, tending towards values more commonly observed for tidal inlets (in the range of 0.85–1.1 (D'Alpaos et al., 2010)). In other words, in the absence of Regime III events, river flow becomes a relatively less important forcing compared to the barotropic forcing in shaping the equilibrium morphology of the estuary. Therefore, in addition to maintaining the long-term morphological equilibrium, Regime III events are also responsible for shaping the morphodynamic equilibrium profile of the estuary.

5.3. *Impact of climate change*

Broadly speaking, the projected impact of climate change relevant for morphological development is two-fold and includes sea level rise (SLR) and changes in river flow rate. SLR in the LPR, under an extreme scenario, is projected to be about 1.3 m (relative to the year 2000) by the year 2070 (Kopp et al., 2019). Although climate change impacts on river flow in the LPR are not known precisely, projections from global climate models generally indicate an increase in total precipitation during storm events. For instance, in the LPR, compared to the historical conditions, total precipitation during a 4-day storm event with a return period of

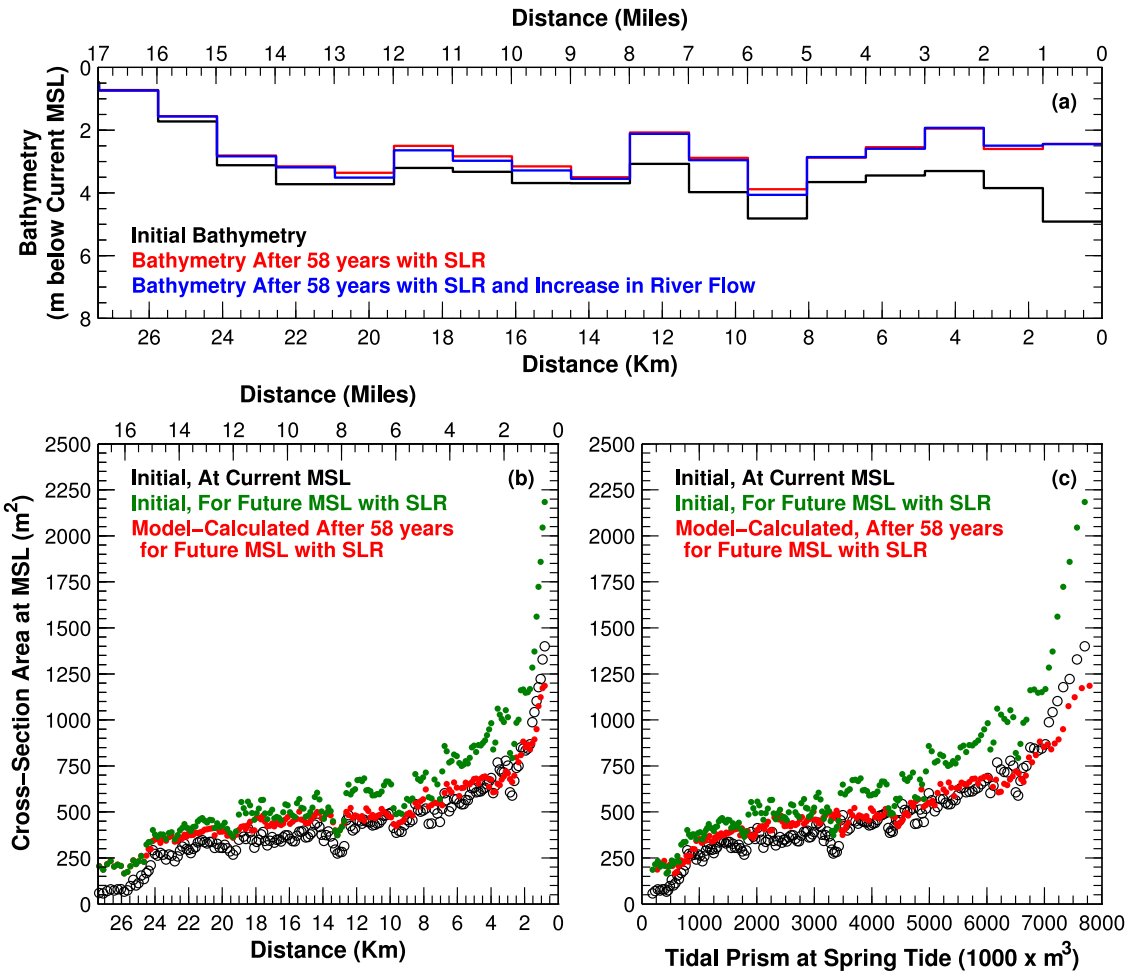

Fig. 13. Application of the morphodynamic model using Morfac to assess the impacts of SLR and increasing river flow due to climate change. Longitudinal profiles of bathymetry – measured in 2007, and model-calculated after 58-year prognostic simulations with SLR and with increasing river flow (a). Longitudinal profiles of cross-sectional area (b), and tidal prism to cross-section relationship (c). Cross-sections in panels b and c shown for current bathymetry at current MSL, current bathymetry for future MSL with SLR, and for calculated bathymetry after a 58-year simulation with SLR.

100 years is projected to increase by about 20% by the year 2080 (CDM Smith, 2019). Therefore, assuming linearity, river flow rate in the future is expected to be higher than current conditions. However, SLR and increasing river flow may have opposing morphological impacts. Specifically, SLR will cause a decrease in currents, thus promoting infilling, whereas increasing river flow will cause an increase in currents, especially during storm events, which could cause erosion and export of sediments from the estuary. Therefore, the relative impact of SLR and increasing river flow was assessed using two incremental prognostic simulations using (1) the projected SLR and current river flow rates, and (2) the projected SLR and projected river flow rates (calculated by enhancing current river flow by 20% as a crude approximation of the additional precipitation due to climate change).

Fig. 13 shows the comparison of initial bathymetry, and calculated bathymetry at the end of the two incremental prognostic simulations. These comparisons show significant infilling over nearly the entire length of the estuary, primarily due to the decrease in currents associated with the increase in water depth due to SLR, and provided sediment loadings are not affected. The results also indicate that SLR rather than increased river flow rate has a greater impact on the morphological evolution of the estuary, with the overall impact of climate change being infill. Possibly, also the sediment load may increase with increasing river flows, which would shorten the time scales to attain the new equilibrium. Since no predictions exist on changes in sediment loading due to climate change, this subject was not addressed in this scenario. Furthermore, the longitudinal profiles of river cross-section and trend of cross-section area with tidal prism shown in Fig. 13 indicate that the estuary adapts to the disequilibrium caused by SLR by infilling and tending towards a morphodynamic profile similar to current conditions (for the current morphology and current MSL) in most of the estuary. However, as seen from localized differences between the cross-section at the end of the prognostic simulation and the cross-section under the current MSL, the 58-year duration of the prognostic simulations is likely not sufficient to attain the equilibrium profile. Nonetheless, the overall response of the system to SLR is consistent with theoretical and historical response to SLR (Meade, 1969).

6. Discussion

The LPR is characterized by predominantly fine sediment transport, although the bed in places is mixed (fines and sands). Consequently, due to memory effects and sediment mobility limitations, transport is below capacity conditions, i.e., no equilibrium exists between the sediment load and the local hydraulic conditions. The amount of mobile sediment, actively forming the river's morphology, is largely influenced by past hydrodynamic conditions, in particular, by episodic erosional events (Mathew and Winterwerp, 2020). The morphodynamic development of the LPR exhibits memory effects at various time scales, from the tidal period to multi-year periods spanning episodic erosional events. At short to intermediate time-scales, the response to hydrodynamic forcing is

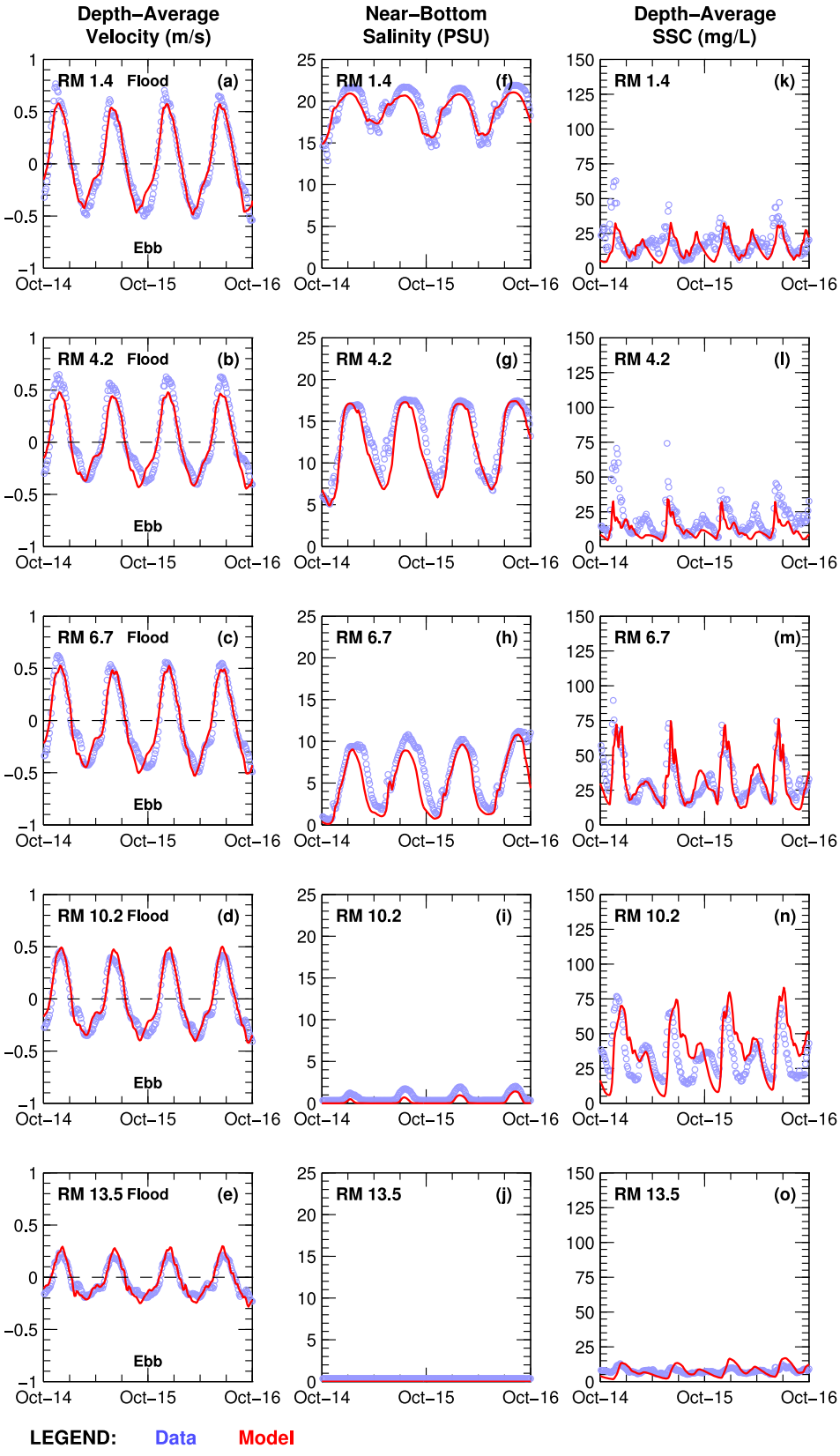

Fig. A.1. Comparison of model performance for (a–e) currents, (f–j) near-bottom salinity, and (k–o) SSC to measurements at the *in situ* moorings in the LPR during low river flow conditions (Regime I).

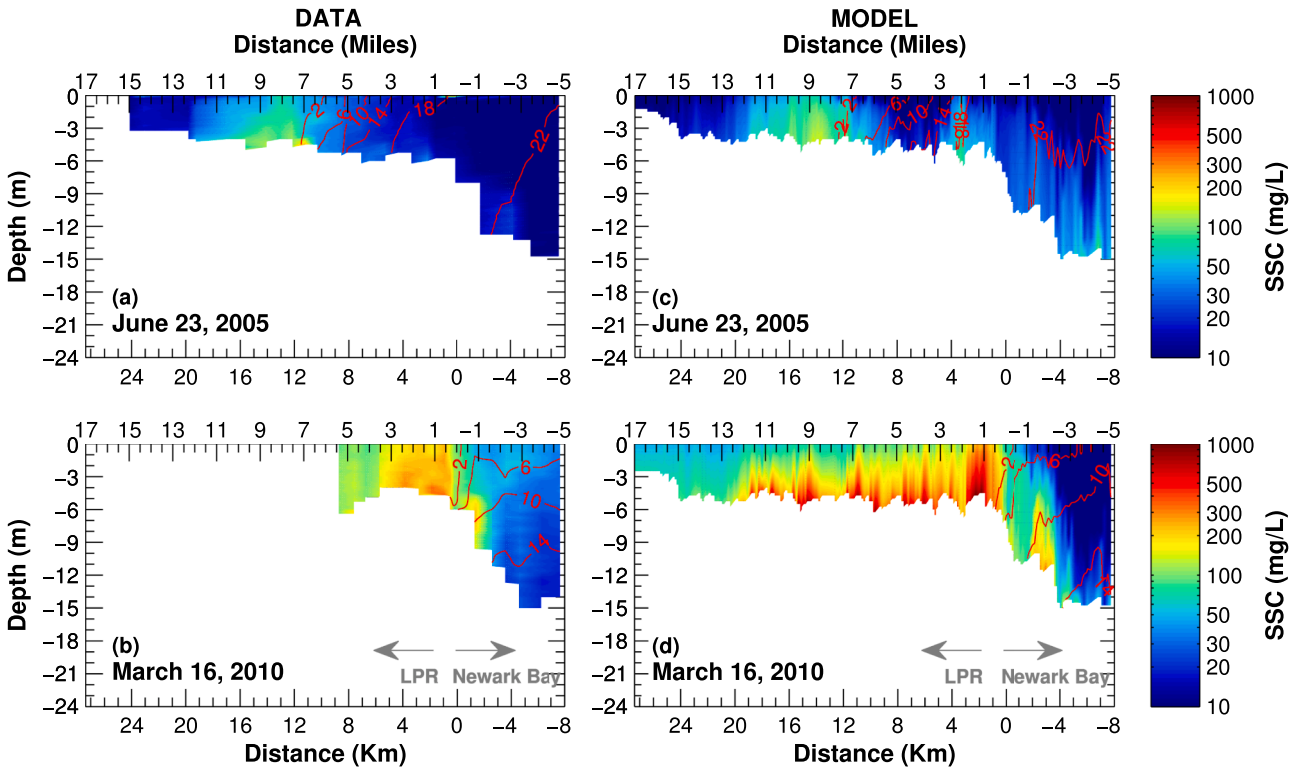

Fig. A.2. Comparison of model performance (c, d) for salinity (contours) and SSC (shaded colors) to along-channel transect measurements (a, b) within the LPR and the navigation channel in Newark Bay during low river flow conditions (Regime I; a and c), and during high river flow conditions (Regime III; b and d).

characterized by three regimes, mainly governed by the river flow and responsible for the morphological response – infilling, flushing and scouring. While quantified for the LPR, this type of system response (i.e., the various transport regimes) is characteristic of fine sediment dynamics in rivers characterized by erosion-limited conditions (Winterwerp et al., 2021, Mathew and Winterwerp, 2020).

The sediment dynamics and its dependency with sediment mobility, memory effects, and consequently, the three transport regimes in the LPR are generally reproduced by the morphodynamic model presented here. The model formulation, specifically the bed schematization with an easily-erodible fluff layer overlying less erodible parent bed subject to consolidation, represents the memory effects on transport, as apparent in the three transport regimes and flow-dependent morphological response. However, the model response is less accurate at local scales, especially for short-term (inter-annual) morphological change. Model performance is limited by the fact that bed composition and stratigraphy cannot be reproduced in detail because they depend on initial conditions and memory effects that are not known precisely. Nonetheless, the model captures the long-term (decadal scale) morphological trend, specifically when the system was under a state of morphological disequilibrium caused by navigational dredging.

The results of the prognostic assessments of shipping, Regime III events, and climate change in the LPR indicate the impact of these forcings in shaping the equilibrium morphology of such systems. Propwash generated by ship propellers can cause erosion, with the location and magnitude of scour dependent on factors such as vessel draft, power applied by the propellers, shipping intensity, etc. In the LPR, this impact is apparent in the erosional signal measured in the reach seaward of RM 2 over the 2007–2008 and 2011–2012 periods, as well as the projected infill of this reach in the prognostic assessment, tending towards an equilibrium profile similar to more landward reaches. Therefore, in the long-term, shipping represents an additional anthropogenic forcing that can influence the equilibrium morphology of such systems. In contrast, episodic Regime III events represents a natural erosional forcing that acts to scour and export sediments accumulating in more landward reaches under Regimes I and II. In the LPR, periods of elevated river flow (resulting in higher bed shear stress) represent such Regime III events, although in other systems, episodic wave events could act in a similar manner. Regime III events shape the equilibrium morphology by maintaining a cross-section that is otherwise deeper than expected based on theory. For instance, hydrologic changes (in the case of the LPR) that impact river flow rate, represents an example of a change in Regime III events that can impact the equilibrium morphology of such systems. Finally, climate change, primarily SLR, is expected to represent a disequilibrium to the system by reducing the magnitude of currents. Consequently, if sediment supply is maintained, the LPR is projected to infill and tend towards the current equilibrium profile (based on cross-section area to tidal prism relationship). Overall, the results of the prognostic assessments of the LPR are conceptually explainable, consistent with theoretical expectations, and indicate the general applicability of the morphodynamic modeling framework (including Morfac) and results. This implies that the modeling framework can be used to assess the long-term and large-scale impacts of issues such as hydrologic changes due to dam construction/removal, changes in navigation, climate change, etc.

The present study indicates that morphological upscaling may be deployed in fine sediment systems between episodic erosional events, provided that morphological upscaling is applied to sediment mass in the bed in order to represent memory effects. The response to episodic erosional events (involving erosion of the parent bed underneath the fluff layer) cannot be represented with the Morfac approach, as this response is too non-linear because of non-linear variations in the availability of mobile sediment. This implies that the morphodynamic modeling of rivers under erosion-limited conditions requires a thorough analysis of the hydrograph, including the recurrence intervals and order of occurrence of the episodic erosional events. These inherent uncertainties are reflected directly in the uncertainties of model predictions, the results of which should therefore be interpreted

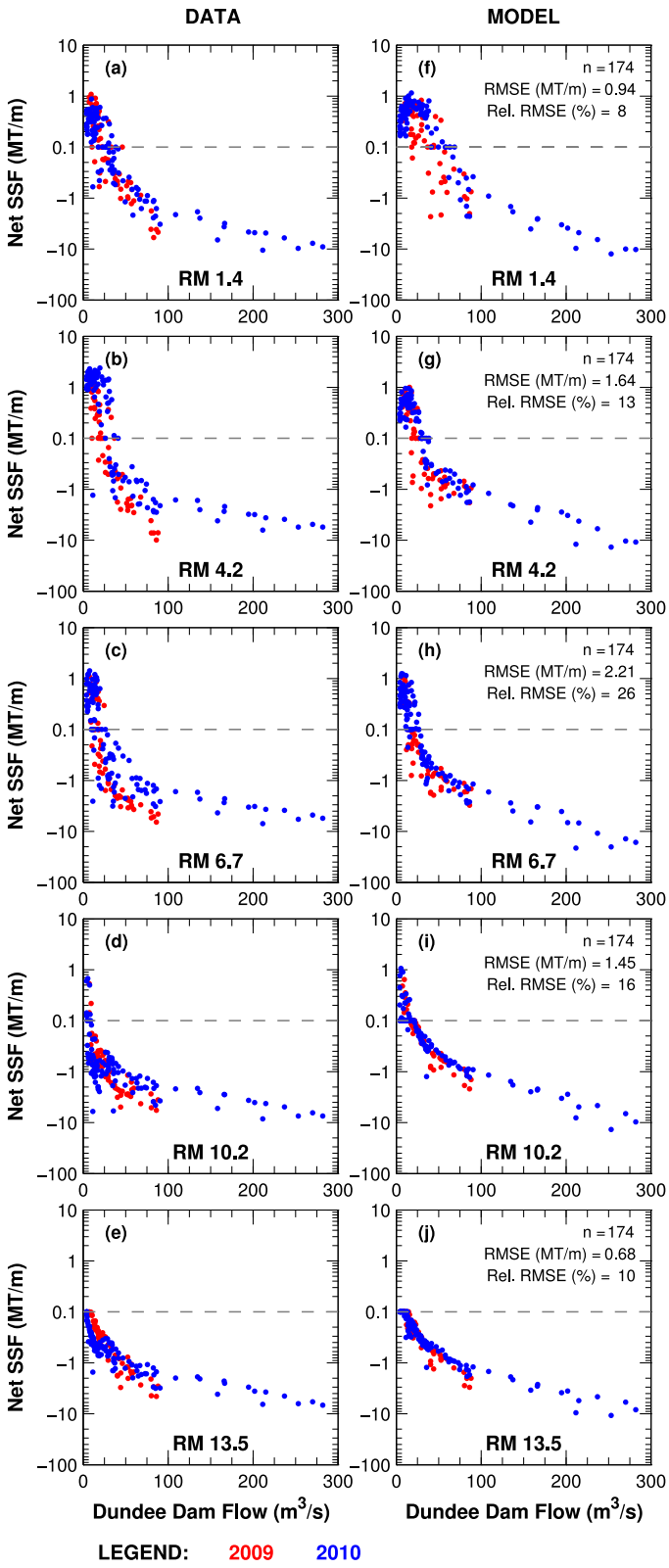

Fig. A.3. Comparison of model performance (f–j) for the trend of SSF versus river flow rate to the measured trend (a–e) at the in situ moorings in the LPR over an extended range of river flows (Regimes I, II, and III). Positive and negative values indicate fluxes directed up-estuary and down-estuary, respectively.

accordingly. When the system is in a state of morphodynamic disequilibrium, the Morfac approach is feasible over the long time scales needed to attain equilibrium.

The model framework presented here, specifically the bed structure for parameterizing and representing erosion-limited conditions, is generally similar to numerical models of such fine sediment systems developed by other authors (van Maren et al., 2015). The model framework is generally applicable to settings with erosion-limited transport associated with either consolidation effects in the bed (e.g., in a purely fine sediment system), or due to armoring in mixed sediment systems. Furthermore, both settings (purely fine sediment and mixed) may occur in the same system, for instance, between the thalweg and adjacent inter-tidal areas. However, such non-linearities driving the system response in fine sediment settings implies that appropriate representation of such systems in morphodynamic models requires a significant amount of site-specific data describing spatial and temporal variations in key transport parameters. These include the erodibility of sediments (for the fluff layer and the parent bed), sediment stratigraphy, temporal trends in erodibility due to consolidation/swelling, and settling velocities for fine sediments in suspension. In practical terms, the relatively large data requirements imply that numerical models of fine sediment systems are almost invariably limited by the availability of data for model parameterization and calibration (Vested et al., 2013).

These considerations indicate the potential for limitations in numerical models of fine sediment systems. While certain limitations (e.g., more spatial discretization of the physical transport processes) may be addressed computationally (e.g., using smaller model grid cells), others require extensive site-specific data. For instance, conceptually, a sediment bed formed by sedimentation in a dredged navigation channel is expected to be more erodible than an undisturbed bed created over millennial timescales. Similarly, a newly deposited sediment bed is expected to consolidate and decrease in erodibility over time. Both effects can be parameterized by appropriate spatially and temporally comprehensive measurements of erodibility. Other limitations may require alternate formulations than traditionally implemented in numerical models. For instance, based on application to data from erosion experiments, (van Prooijen and Winterwerp, 2010) propose a formulation that includes a Gaussian distribution of turbulent bed shear stress, a stochastic distribution of τ_{Cr} and using dozens of fine sediment classes. In contrast, typical model formulations characterize the turbulence-mean shear stress at the bed-water interface and parameterize the mean critical shear stress along with one or, at most, a few fine sediment classes.

Finally, another conceptual and philosophical aspect to consider is that models are schematized and simplified representations of reality. Model performance responds to the numerical parameterization of various processes that may introduce deviations from reality over the long-term. In other words, the model has its own equilibrium which may or may not be identical to reality. Such limitations and related uncertainties require consideration when assessing model performance. For the application presented in this paper, the primary uncertainty is in its performance over the short term and over small spatial scales. Model performance over the long term and large spatial scales is comparable to data. Therefore, the morphodynamic model framework including the Morfac approach presented here is concluded to be suitable for assessing the long-term and large-scale morphodynamics in fine sediment settings where memory effects and sediment mobility have a strong influence on transport and morphological development. However, details such as the flow thresholds for periods with and without morphological acceleration, the value of f_{mor}, etc., are system-specific and require careful assessment for appropriate representation.

7. Conclusions

Morphodynamics of fine sediment systems differ in several key respects from sandy systems. In addition to being dependent upon the

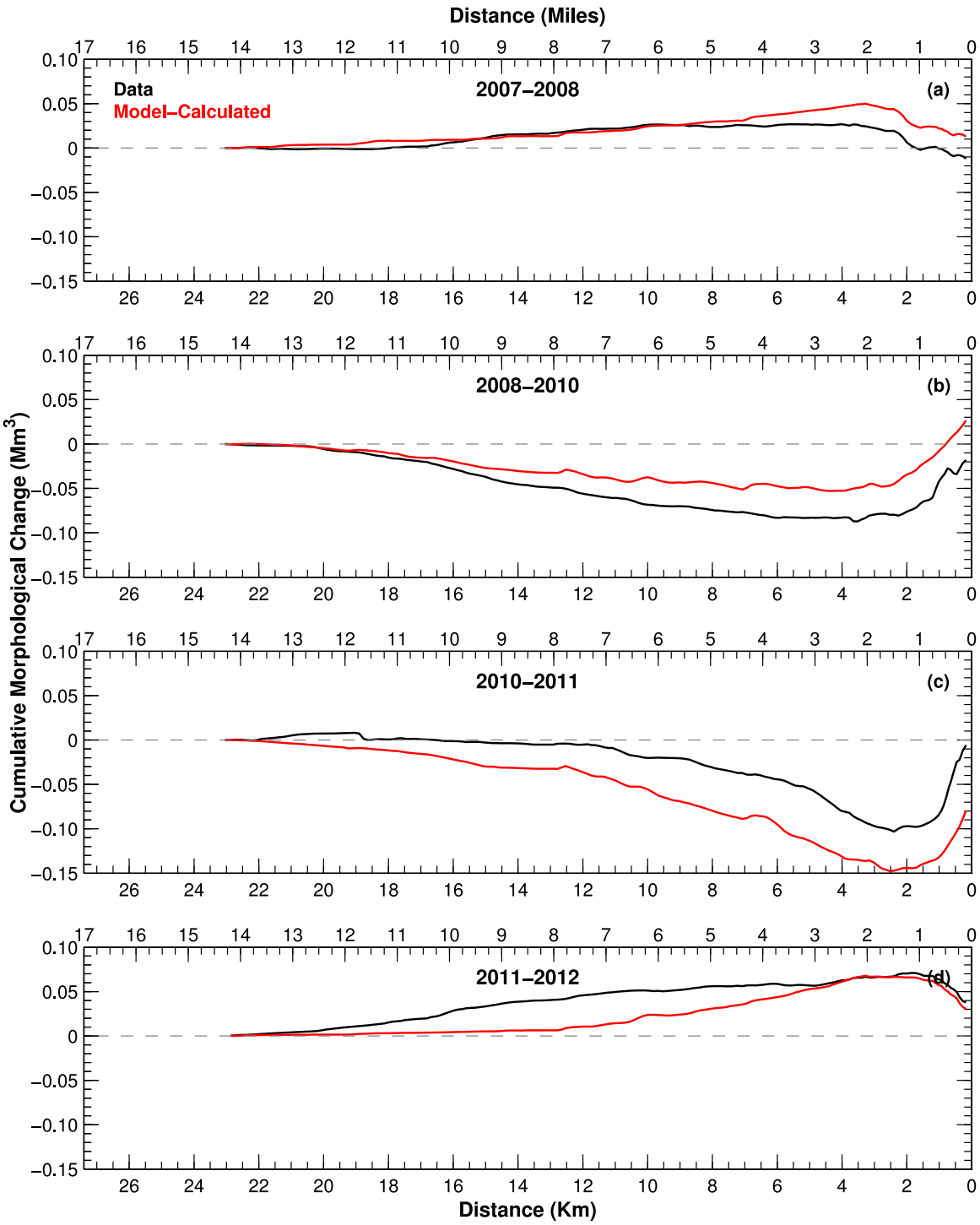

Fig. A.4. Comparison of measured and model-calculated longitudinal profile of cumulative (in the seaward direction) volumetric morphological change in the LPR. Positive slope indicates deposition and negative slope indicates erosion. Morphological change over the (a) 2007–2008, (b) 2008–2010, (c) 2010–2011, and (d) 2011–2012 survey periods.

external forcings (which is the case also in sandy systems), morphodynamics in fine sediment systems are also a consequence of non-equilibrium transport related to sediment mobility and memory effects induced by the time-history of morphological development. These processes were assessed empirically and used to develop a conceptual picture of sediment dynamics and transport regimes in the LPR (Mathew and Winterwerp, 2020) and generally reproduced by the morphodynamic model application presented in this paper. Furthermore, morphological upscaling following the Morfac approach, and using formulations specifically adapted for fine sediment settings, is shown to be an appropriate tool for computationally efficient long-term morphodynamic modeling in such systems. The morphodynamic model framework using Morfac presented here provides a tool for assessing the long-term morphodynamics in fine sediment systems for applications such as the design and impact of engineering interventions (e.g., dredging, river training works, etc.), impact of climate change, development of sediment management strategies, etc.

CRediT authorship contribution statement

Rooni Mathew: Conceptualization, Methodology, Software, Validation, Formal analysis, Resources, Data curation, Writing – original draft, Writing – review & editing, Visualization, Project administration. **Johan C. Winterwerp:** Conceptualization, Methodology, Formal analysis, Writing – review & editing.

Declaration of Competing Interest

The authors declare that they have no known competing financial interests or personal relationships that could have appeared to influence the work reported in this paper.

Acknowledgment

This research did not receive any specific grant from funding agencies in the public, commercial, or not-for-profit sectors. The data used in this paper was collected as part of the Remedial Investigation of the Lower Passaic River Study Area being conducted by the Cooperating Parties Group under supervision by the United States Environmental Protection Agency and are available at http://www.ourpassaic.org. Similarly, the overall modeling framework is open source and available for download at https://www.hdrinc.com/services/environmental-sciences/water-quality-hydrodynamic-modeling-software. The code version including the specific capabilities developed in this paper (the fluff layer, morphological upscaling, etc.) may be obtained by a direct request to the primary author. Furthermore, the information in this paper does not necessarily reflect the views of the United States Environmental Protection Agency and no official endorsement should be inferred.

Appendix A

Model calibration performance was assessed relative to various metrics including currents, salinity, SSC, SSF, and morphological change. Fig. A.1 shows a comparison of model performance relative to the measured depth-average velocity, near-bottom salinity, and depth-average SSC at the in situ moorings (locations shown in Fig. 1) over October 14–15, 2009 when river flow rate at Dundee Dam averaged 8 m^3/s (Regime I, infilling conditions). During this period, the model reproduces several key features apparent in the data:

- Tidal asymmetry (flood dominance) in currents.
- The magnitude and intra-tidal trends in salinity and SSC.
- The location of the salt front generally in the reach between RM 6.7 and RM 10.2.
- Increasing SSC in the up-estuary direction, with maximum SSC generally in the reach between RM 6.7 and RM 10.2. In combination with the location of the salt front in this reach, this is indicative of the ETM location, and SSC dynamics within the ETM.
- The effect of tidal asymmetry on SSC, primarily manifest as higher SSC during flood than during ebb.
- Relatively low SSC and relatively low intra-tidal variability in SSC at the freshwater tidal station (RM 13.5), which is an indication of solids with relatively lower settling velocity entering from the head-of-tide. This is in contrast to the locations within the salt wedge (RM 1.4, RM 4.2, RM 6.7) which experience higher intra-tidal variability in SSC and indicative of solids with relatively higher settling velocity. These spatially varying dynamics are reproduced by the model primarily by having higher settling velocity for solids originating from marine sources as compared to the freshwater sources.

Model performance was also assessed using along-channel transects of water depth, salinity, and SSC within the LPR and within the navigation channel in Newark Bay. Fig. A.2 shows such a comparison for June 23, 2005 and March 16, 2010 when river flow rate at Dundee Dam averaged 8 m^3/s (Regime I conditions) and 450 m^3/s (Regime III; return period of 25-years), respectively. Within the LPR, the model reproduces major features in the data such as the salt front and its location, and the presence of the ETM associated with the salt front. In addition, the model reproduces the difference in SSC values within the ETM between the two events, with higher SSC during the March 16, 2010 event as compared to the June 23, 2005 event.

The measurements of velocity and SSC at the *in situ* moorings were used to calculate the tidally-integrated net SSF at these locations over the years 2009 and 2010. The resulting net SSF shows a relationship with river flow rate as seen from the left panels in Fig. A.3, a trend that is reproduced by the model as seen in the right panels of Fig. A.3. Statistical metrics quantifying the model-data comparisons are also included – these include the root mean square error (RMSE), a measure of the error between the model and data as expressed by:

$$RMSE = \sqrt{\frac{\sum \left(SSF_{Data} - SSF_{Model}\right)^2}{n}} \tag{A.1}$$

where SSF_{Data} = measured tidally-integrated SSF, SSF_{Model} = model-calculated tidally-integrated SSF, and n = number of pairs of model and data. Another metric quantifying the model-data performance is the relative RMSE (%), defined as the RMSE relative to the data range (the difference between the minimum and maximum measured value). Within the predominantly estuarine locations (RM 1.4, RM 4.2, and RM 6.7), low river flows are associated with net up-estuary SSF, with net down-estuary SSF as river flow increases. In contrast, net SSF at the freshwater tidal location (RM 13.5) is consistently directed down-estuary. At RM 1.4, during river flows ranging between about 30-150 m^3/s model performance is somewhat inconsistent with data – the magnitude of net SSF tends to be biased low compared to the data. Assessment of model performance at RM 4.2 and RM 6.7 over this range of flow rates shows a similar bias at these locations as well. This suggests that the model does not calculate enough erosion in the more landward reaches of the LPR. This limitation in model performance may partly be related to the time-history of events and the ability of the model to capture variations in sediment erodibility at small spatial and temporal scales – this is one of the difficulties involved in modeling fine sediment transport in such erosion-limited settings. Furthermore, as indicated by Mathew and Winterwerp (2020), erosion during such conditions, which are nominally representative of Regime II, is limited to the fluff layer (and the transition layer) and is therefore less significant from a morphological perspective as compared to Regimes I and III.

The comparison of large-scale flow-dependent morphological trends is seen more clearly in Fig. A.4, which shows the measured and model-calculated cumulative (starting from the landward end) volumetric morphological change over the various time-periods. Overall trends are

consistent between the model and data – landward of RM 2, the model reproduces the depositional trends in 2007-2008 and 2011-2012, and the erosional trends in 2008-2010 and 2010-2011. Similarly, seaward of RM 2, the model reproduces the depositional trends in 2008-2010 and 2010-2011 (as mentioned previously, the erosional trend seaward of RM 2 during 2007-2008 and 2011-2012 is driven by the parameterized shipping scour process). During the low-flow periods (2007-2008 and 2011-2012), the model-calculated magnitude of infill landward of RM 2 is comparable to the data. However, model performance of erosion landward of RM 2 during the high-flow periods (2008-2010 and 2010-2011) is more variable, with a bias towards under-prediction during the former period and over-prediction during the latter period Eq. (A1).

Potential explanations why the model does not capture local-scale changes over inter-annual scales include limitations related to various model inputs and formulations:

- Bed initial conditions – The core profile measurements used to define model initial conditions are somewhat sparse and do not capture the full range of spatial and depth-dependent heterogeneity. Moreover, they do not necessarily match the equilibrium solution of the model.
- Erodibility – The available data for erodibility of the parent bed were conducive to the development of only a single set of erodibility inputs over the entire LPR which is likely to be a simplification of the spatial heterogeneity in reality. Moreover, these may vary over time inducing the memory effects discussed in Section 1.
- Grid resolution – The resolution of the model grid, limited by computation time, is not sufficient to resolve small-scale features such as bridge support pillars, shoreline structures, etc., which cause local scour during high river flow events, with infill of the scoured areas during low river flow conditions.
- Shipping-induced scour – The exact timing and magnitude of this source term is unknown. For the model simulations presented here, the locations of scour and scour rate were parameterized using the measured bathymetry, and the scour rate was assumed to be constant in time, all of which are simplified representations of the process.
- Consolidation time-scales – Consolidation time-scales and their impact on erodibility are not very well characterized, both generally as well as specifically in the case of the LPR. For instance, at initialization, the model assumes that sediments in the bed to be fully consolidated (and therefore, less erodible) whereas in reality, some surficial sediments may be newly deposited and not fully consolidated (i.e., more erodible).
- Flocculation effects – Although the model includes parameterized approximations of flocculation effects on settling velocity, it does not capture the full range of spatial and temporal heterogeneity of this process, neither in the sediment bed, nor in the water column. For example, the model only includes two representative floc classes, whereas in reality, floc sizes and settling velocities are expected to vary over large range.

References

Blumberg, A.F., Mellor, G.L., 1978. A coastal ocean numerical model (Eds.). In: Sündermann, J., Holz, K.P. (Eds.), Mathematical Modelling of Estuarine Physics. Springer-Verlag, New York. https://doi.org/10.1029/LN001p0203.

Borrowman, T.D., Smith, E.R., Gailani, J.Z., Caviness, L., 2006. Erodibility Study of Passaic River Sediments using USACE Sedflume. US Army Engineer Research and Development Center, Vicksburg, MS, USA.

CDM Smith, Matrix new world, Passaic river basin climate resilience planning study, Prepared for the North Jersey Transportation Planning Authority, Newark, NJ, USA, 2019.

Cheng, N.A., 1997. Simplified settling velocity formula for sediment particles. J. Hydraul. Eng. 123, 149–152.

D'Alpaos, A., Lanzoni, S., Marani, M., Rinaldo, A., 2010. On the tidal prism–channel area relations. J. Geophys. Res. 115, F01003. https://doi.org/10.1029/2008JF001243.

Dam, G., van der Wegen, M., Labeur, R.J., Roelvink, D., 2016. Modeling centuries of estuarine morphodynamics in the Western Scheldt estuary. Geophys. Res. Lett. 43, 3839–3847. https://doi.org/10.1002/2015GL066725.

Dronkers, J., 2017. Convergence of estuarine channels. Cont. Shelf Res. 144, 120–133. https://doi.org/10.1016/j.csr.2017.06.012.

Frings, R.M., Ottevanger, W., (C.J.) Sloff, K., 2011. Downstream fining processes in sandy lowland rivers. J. Hydraul. Res. 49, 178–193. https://doi.org/10.1080/00221686.2011.561000.

Ganju, N.K., Schoellhamer, D.H., Jaffe, B.E., 2009. Hindcasting of decadal-timescale estuarine bathymetric change with a tidal-timescale model. J. Geophys. Res. 114, F04019. https://doi.org/10.1029/2008JF001191.

George, D.A., Gelfenbaum, G., Stevens, A.W., 2012. Modeling the hydrodynamic and morphologic response of an estuary restoration. Estuar. Coast. 35, 1510–1529. https://doi.org/10.1007/s12237-012-9541-8.

Gessler, J., 1967. The Beginning of Bedload Movement of Mixtures Investigated as Natural Armoring in Channels. California Institute of Technology, Pasadena CA.

Geyer, W.R., Woodruff, J.D., Traykovski, P., 2001. Sediment transport and trapping in the Hudson River estuary. Estuaries 24, 670–679.

HydroQual, 2008. Final Hydrodynamic Modeling Report, Lower Passaic River Restoration Project and Newark Bay Study. U.S. Environmental Protection Agency, Mahwah, NJ, USA. Prepared for.

HydroQual, Inc., 2010. A primer for ECOMSED Version 1.4-LPR: Users Manual. HydroQual, Inc., Mahwah, NJ.

Kopp, R.E., Andrews, C., Broccoli, A., Garner, A., Kreeger, D., Leichenko, R., Lin, N., Little, C., Miller, J.A., Miller, J.K., Miller, K.G., Moss, R., Orton, P., Parris, A., Robinson, D., Sweet, W., Walker, J., Weaver, C.P., White, K., Campo, M., Kaplan, M., Herb, J., Auermuller, L. New Jersey's rising seas and changing coastal storms: report of the 2019 science and technical advisory panel, Prepared for the New Jersey Department of Environmental Protection. Trenton, NJ, USA, 2019.

Lesser, G.R., Roelvink, J.A., van Kester, J.A.T.M., Stelling, G.S., 2004. Development and validation of a three-dimensional morphological model. Coast. Eng. 51, 883–915.

Lesser, G.R. An approach to medium-term coastal morphological modelling, PhD thesis, UNESCO-IHE & Delft Technical University, Delft, The Netherlands, ISBN 978-0-415-55668-2. 2009.

Mathew, R., Winterwerp, J., 2017. Surficial sediment erodibility from time-series measurements of suspended sediment concentrations: development and validation. Ocean Dyn. 67, 691–712. https://doi.org/10.1007/s10236-017-1055-2.

Mathew, R., Winterwerp, J., 2020. Sediment dynamics and transport regimes in a narrow microtidal estuary. Ocean Dyn. 70, 435–462. https://doi.org/10.1007/s10236-020-01345-9.

Meade, R.H., 1969. Landward transport of bottom sediments of the Atlantic coastal plain. J. Sediment Petrol. 39, 222–234.

Mehta, A.J., 1988. Laboratory studies on cohesive sediment deposition and erosion (Eds). In: Dronker, J., van Leussen, W. (Eds.), Physical Processes in Estuaries. Springer, Berlin, pp. 427–445.

Mellor, G.L., Yamada, T., 1982. Development of a turbulence closure model for geophysical fluid problems. Rev. Geophys. Space Phys. 20, 851–875.

Moffatt Nichol, Deltares, Appendix M: Sediment transport model of the Lower Passaic river, Lower Passaic River RI/FS, New York, NY, USA, 2019.

Partheniades, E., 1965. Erosion and deposition of cohesive soils. J. Hydraul. Div. ASCE 91, 105–139.

Ranasinghe, R., Swinkels, C.M., Luijendijk, A.P., Roelvink, J.A., Bosboom, J., Stive, M.J. F, Walstra, D.J.R, 2011. Morphodynamic upscaling with the MORFAC approach: dependencies and sensitivities. Coast. Eng. 58, 806–811. https://doi.org/10.1016/j.coastaleng.2011.03.010.

Roberts, J., Jepsen, R., Gotthard, D., Lick, W., 1998. Effects of particle size and bulk density on erosion of quartz particles. J. Hydraul. Eng. 124, 1261–1267.

Roelvink, J.A., 2006. Coastal morphodynamic evolution techniques. Coast. Eng. 53, 277–287.

Sanford, L.P., Maa, J.P.Y., 2001. A unified erosion formulation for fine sediments. Mar. Geol. 179, 9–23.

Sanford, L.P., 2008. Modeling a dynamically varying mixed sediment bed with erosion, deposition, bioturbation, consolidation, and armoring. Comput. Geosci. 34, 1263–1283.

Sea Engineering, Sedflume analysis data report, Newark Bay, New Jersey, Prepared for U.S. Environmental Protection Agency, Santa Cruz, CA, USA, 2013.

Smagorinsky, J., 1963. General circulation experiments with the primitive equations, I. The basic experiment. Mon. Weather Rev. 91, 99–164.

Styles, R., Brown, M.E., Brutsche, K.E., Li, H., Beck, T.M., Sanchez, A., 2016. Long-term morphological modeling of barrier island tidal inlets. J. Mar. Sci. Eng. 4, 65.

Sutherland, J., Peet, A.H., Soulsby, R.L., 2004. Evaluating the performance of morphological models. Coast. Eng. 51, 917–939.

Tran, D., Strom, K., 2019. Floc sizes and resuspension rates from fresh deposits: Influences of suspended sediment concentration, turbulence, and deposition time. Estuar. Coast Shelf S. 229, 106397.

U.S. Army Corps of Engineers, Geomorphological/geophysical characterization of the nature and dynamics of sedimentation and sediment transport in newark bay focusing on the effects related to continued and future federal navigation channel deepening and maintenance, New York, NY, USA, 2006.

U.S. Army Corps of Engineers, 2010. Lower Passaic River Commercial Navigation Analysis. U.S. Army Corps of Engineers, New York, NY, USA.

van der Wegen, M., Jaffe, B.E., 2014. Processes governing decadal-scale depositional narrowing of the major tidal channel in San Pablo Bay, California, USA. J. Geophys. Res. Earth Surf. 119, 1136–1154. https://doi.org/10.1002/2013JF002824.

van der Wegen, M., Roelvink, J.A., 2008. Long-term morphodynamic evolution of a tidal embayment using a two-dimensional, process-based model. J. Geophys. Res. 113, C03016. https://doi.org/10.1029/2006JC003983.

van Maren, D.S., van Kessel, T., Cronin, K., Sittoni, L., 2015. The impact of channel deepening and dredging on estuarine sediment concentration. Cont. Shelf. Res. 95, 1–14. https://doi.org/10.1016/j.csr.2014.12.010.

van Prooijen, B.C., Winterwerp, J.C., 2010. A stochastic formulation for erosion of cohesive sediments. J. Geophys. Res. 115, C01005. https://doi.org/10.1029/2008JC005189.

van Rijn, L.C., Walstra, D.J.R., Grasmeijer, B., Sutherland, J., Pan, S., Sierra, J.P., 2003. The predictability of crossshore bed evolution of sandy beaches at the time scale of storms and seasons using process-based profile models. Coast. Eng. 47, 295–327.

van Rijn, L.C., 1993. Principles of Sediment Transport in Rivers, Estuaries and Coastal Seas. Aqua Publications, Amsterdam.

Vested, H.J., Tessier, C., Christensen, B.B., Goubert, E., 2013. Numerical modelling of morphodynamics – Vilaine Estuary. Ocean Dyn. 63, 423–446. https://doi.org/10.1007/s10236-013-0603-7.

Winterwerp, J.C., van Kesteren, W.G.M., 2004. Introduction to the Physics of Cohesive Sediment in the Marine Environment. Elsevier, Amsterdam.

Winterwerp, J.C., Van Kessel, T., Van Maren, B.S., Van Prooijen, B.C., 2021. Fine Sediment in Open Water – From Fundamentals to Modeling. World Scientific. https://doi.org/10.1142/12473.

Winterwerp, J.C., 2002. On the flocculation and settling velocity of estuarine mud. Cont. Shelf Res. 22, 1339–1360.